Journal of Sound and Vibration 328 (2009) 259–290

Contents lists available at ScienceDirect

Journal of Sound and Vibration

journal homepage: www.elsevier.com/locate/jsvi

2-D differential quadrature solution for vibration analysis of functionally graded conical, cylindrical shell and annular plate structures

Francesco Tornabene [a], Erasmo Viola [a,*], Daniel J. Inman [b]

[a] DISTART Department, Faculty of Engineering, University of Bologna, Italy
[b] Center of Intelligent Material Systems and Structures, Virginia Polytechnic Institute and State University, USA

ARTICLE INFO

Article history:
Received 11 December 2007
Received in revised form
12 June 2009
Accepted 24 July 2009
Handling Editor: A.V. Metrikine
Available online 10 September 2009

ABSTRACT

This paper focuses on the dynamic behavior of functionally graded conical, cylindrical shells and annular plates. The last two structures are obtained as special cases of the conical shell formulation. The first-order shear deformation theory (FSDT) is used to analyze the above moderately thick structural elements. The treatment is developed within the theory of linear elasticity, when materials are assumed to be isotropic and inhomogeneous through the thickness direction. The two-constituent functionally graded shell consists of ceramic and metal that are graded through the thickness, from one surface of the shell to the other. Two different power-law distributions are considered for the ceramic volume fraction. The homogeneous isotropic material is inferred as a special case of functionally graded materials (FGM). The governing equations of motion, expressed as functions of five kinematic parameters, are discretized by means of the generalized differential quadrature (GDQ) method. The discretization of the system leads to a standard linear eigenvalue problem, where two independent variables are involved without using the Fourier modal expansion methodology. For the homogeneous isotropic special case, numerical solutions are compared with the ones obtained using commercial programs such as Abaqus, Ansys, Nastran, Straus, Pro/Mechanica. Very good agreement is observed. Furthermore, the convergence rate of natural frequencies is shown to be very fast and the stability of the numerical methodology is very good. Different typologies of non-uniform grid point distributions are considered. Finally, for the functionally graded material case numerical results illustrate the influence of the power-law exponent and of the power-law distribution choice on the mechanical behavior of shell structures.

1. Introduction

Thin and thick shells have been widespread in many fields of engineering because they give rise to optimum conditions for dynamic behavior, strength and stability. These structures support applied external forces efficiently by virtue of their geometrical shape. In other words, shells are much stronger and stiffer than other structural shapes. The vibration effects on shell structures caused by different phenomena can be of serious consequence for their strength and safety. Therefore, an accurate frequency and mode shape determination is of considerable importance for the technical design of these structural elements.

* Corresponding author. Tel.: +39 051 209 3510; fax: +39 051 209 3495.
E-mail address: erasmo.viola@mail.ing.unibo.it (E. Viola).

0022-460X/$ - see front matter © 2009 Elsevier Ltd. All rights reserved.
doi:10.1016/j.jsv.2009.07.031

As for many other shape kinds, conical, cylindrical shells and annular plates are very common structural elements. So, the purpose of this paper is to study the dynamic behavior of these structures derived from shells of revolution.

There are various 2-D theories of thin shells, which are used to approximate the real 3D problem. In the last 50 years, refined 2-D linear theories of thin shells have been developed including important contributions by Sanders [1], Flügge [2], Novozhilov [3], Vlasov [4], Kraus [5], Leissa [6] and Niordson [7]. In these refined shell theories, deformation is based on the Kirchhoff-Love assumption. Based on the Kirchhoff-Love shell theory, named classical shell theory (CST), many researches analyzed various characteristics of thin conical shell structures [8–15].

Simple and accurate theories for thick shells have been developed [5,16–18]. With respect to thin shells, the thick shell theories take the transverse shear deformation and rotary inertia into account. The transverse shear deformation has been incorporated into shell theories by following the work of Reissner [19]. The present work is just based on the first-order shear deformation theory. The geometric model refers to a moderately thick shell, and the effects of transverse shear deformation as well as rotary inertia are taken into account. Several studies have been presented earlier for the vibration analysis of such revolution shells and the most popular numerical tool in carrying out these analyses is currently the finite element method [16–18]. The generalized collocation method based on the ring element method has also been applied. With regard to the latter method, each static and kinematic variable is transformed into a theoretically infinite Fourier series of harmonic components, with respect to the circumferential coordinates [20–23]. In a panel, however, it is not possible to perform such a reduction operation, and the 2-D field must be dealt with directly. In this paper, the governing equations of motion are a set of five 2-D partial differential equations with variable coefficients. These fundamental equations are expressed in terms of kinematic parameters and can be obtained by combining the three basic sets of equations, namely balance, congruence and constitutive equations.

Referring to the formulation of dynamic equilibrium in terms of harmonic amplitudes of mid-surface displacements and rotations, in this paper the system of second-order linear partial differential equations is solved without resorting to the 1-D formulation of the dynamic equilibrium of the shell. Now, the discretization of the system leads to a standard linear eigenvalue problem, where two independent variables are involved. In this way, it is possible to compute the complete assessment of the modal shapes corresponding to natural frequencies of panel structures. It should be noted that there is comparatively little literature available for these structures, compared to literature on the free vibration analysis of complete shells of revolution. Complete revolution shells are obtained as special cases of shell panels by satisfying the kinematic and physical compatibility at the common meridian with $\vartheta = 0, 2\pi$.

As regards material advances, functionally graded materials (FGM) are a class of composites that have a smooth and continuous variation of material properties from one surface to another and thus can alleviate stress concentrations found in laminated composites.

In this study, ceramic–metallic graded shells of revolution with two different power-law variations of the volume fraction of constituents in the thickness direction are considered. The effect of the power-law exponent and distribution choice on the mechanical behavior of functionally graded shells is investigated. Some researchers analyzed various characteristics of functionally graded structures [18,24–36]. However, this paper is motivated by the lack of studies found in the literature addressing to the free vibration analysis of functionally graded conical, cylindrical shells and annular plates and to the effect of the power-law distribution choice on their mechanical behavior.

The solution is obtained by using the numerical technique termed generalized differential quadrature (GDQ) method, which leads to a generalized eigenvalue problem. The main features of the numerical technique under discussion are illustrated in Section 3, while mathematical fundamentals and recent developments of the GDQ method as well as its major applications in engineering are discussed in detail by Shu [37]. The solution is given in terms of generalized displacement components of the points lying on the middle surface of the shell. Then, in order to verify the accuracy of this method, numerical results for the isotropic and homogeneous material case will also be computed by using commercial programs. Different typologies of grid point distribution are also considered, and their effect on solution accuracy is investigated. The convergence and stability of some natural frequencies for the considered structures with different boundary conditions are reported. For the worked out examples, the approximate solutions show good convergence characteristics and appear to be accurate when tested by comparison with each other.

It can be pointed out that in this paper the numerical statement of the problem does not involve any variational formulation, but deals directly with the governing equations of motion, which are directly transformed in one step to obtain the final algebraic form. Moreover, a linear eigenvalue problem involving two independent variables over a 2-D domain is solved. As shown in the literature [38–43], the GDQ technique is a global method, which can obtain very accurate numerical results by using a considerably small number of grid points.

2. Basic governing equations

2.1. Shell geometry and kinematic equations

The geometry of shells considered hereafter is a surface of revolution. The notation for the coordinates is shown in Fig. 1 for a generic conical shell. The coordinates along the meridional and circumferential directions are x and s, respectively. α is a semi-vertex angle of the cone while R_b is the shift of the axis x_3' with reference to the axis of revolution x_3. The distance of

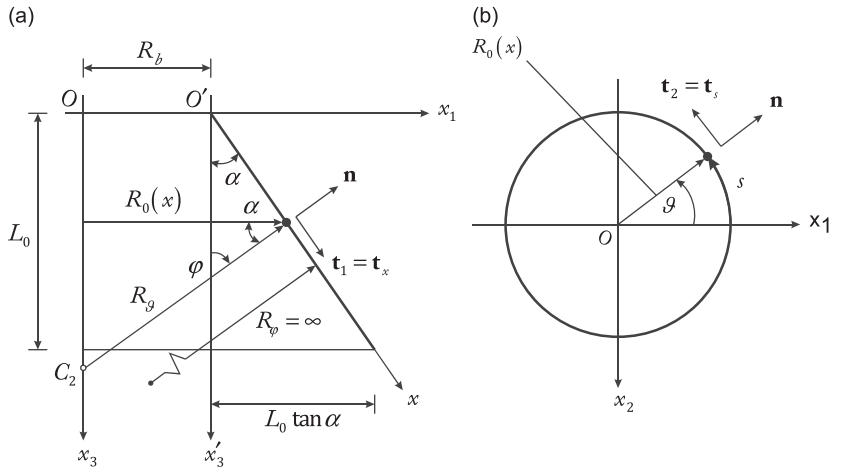

Fig. 1. Coordinate system of the shell: meridional section (a) and circumferential section (b).

each point from the axis of revolution x_3 is $R_0(x)$ and $\varphi = \pi/2 - \alpha$ is the angle between the normal to the shell surface **n** and the axis x_3'. The total thickness of the shell is represented by h. The distance of each point from the shell mid-surface along the normal is ζ.

The position of an arbitrary point within the shell material is known by the coordinates $x\,(0 \le x \le x_0 = L_0/\cos\alpha)$, $s\,(0 \le s \le s_0(x) = \vartheta R_0(x))$ upon the middle surface, and ζ directed along the outward normal **n** and measured from the reference surface $(-h/2 \le \zeta \le h/2)$.

R_φ and R_ϑ are, in general case, the radii of curvature in the meridional and circumferential directions, respectively. For a cone surface we have $R_\varphi = \infty$ and $R_\vartheta = R_0/\sin\varphi$. The horizontal radius $R_0(x)$ of a generic parallel of the shell represents the distance of each point from the axis of revolution x_3 and assumes the form:

$$R_0(x) = R_b + x\sin\alpha = R_b + x\cos\varphi \tag{1}$$

The parametric coordinates (x, s) are defined on the meridional lines and on the parallel circles upon the middle surface of the shell, respectively. It is worth noting that, by vanishing the semi-vertex angle α $(\alpha = 0)$, we can reduce the formulation of conical shells to that of cylindrical shells, while we can obtain the formulation of annular panels and plates, when $\alpha = \pi/2$.

In developing a moderately thick shell theory we make certain assumptions. They are outlined below:

- The transverse normal is inextensible:

$$\varepsilon_n \approx 0$$

- Normals to the reference surface of the shell before deformation remain straight, but not necessarily normal after deformation (a relaxed Kirchhoff-Love hypothesis).
- The transverse normal stress is negligible so that the plane assumption can be invoked:

$$\sigma_n = \sigma_n(x, s, \zeta, t) = 0$$

where t is the time variable.

Consistent with the assumptions of a moderately thick shell theory, the displacement field assumed in this study is that of the *first-order shear deformation theory* and can be put in the following form:

$$U_x(x, s, \zeta, t) = u_x(x, s, t) + \zeta\beta_x(x, s, t)$$

$$U_s(x, s, \zeta, t) = u_s(x, s, t) + \zeta\beta_s(x, s, t)$$

$$W(x, s, \zeta, t) = w(x, s, t) \tag{2}$$

where u_x, u_s, w are the displacement components of points lying on the middle surface $(\zeta = 0)$ of the shell, along meridional, circumferential and normal directions, respectively. β_x and β_s are normal-to-mid-surface rotations, respectively. The kinematics hypothesis expressed by Eqs. (2) should be supplemented by the statement that the shell deflections are small and strains are infinitesimal, that is $w(x, s, t) \ll h$.

It is worth noting that in-plane displacements U_x and U_s vary linearly through the thickness, while W remains independent of ζ. Relationships between strains and displacements along the shell reference (middle) surface $\zeta = 0$ are

represented by the following:

$$\varepsilon_x^0 = \frac{\partial u_x}{\partial x}, \quad \varepsilon_s^0 = \frac{\partial u_s}{\partial s} + \frac{u_x \cos\varphi}{R_0} + \frac{w \sin\varphi}{R_0}, \quad \gamma_{xs}^0 = \frac{\partial u_s}{\partial x} + \frac{\partial u_x}{\partial s} - \frac{u_s \cos\varphi}{R_0}$$

$$\chi_x = \frac{\partial \beta_x}{\partial x}, \quad \chi_s = \frac{\partial \beta_s}{\partial s} + \frac{\beta_x \cos\varphi}{R_0}, \quad \chi_{xs} = \frac{\partial \beta_s}{\partial x} + \frac{\partial \beta_x}{\partial s} - \frac{\beta_s \cos\varphi}{R_0}$$

$$\gamma_{xn} = \frac{\partial w}{\partial x} + \beta_x, \quad \gamma_{sn} = \frac{\partial w}{\partial s} - \frac{u_s \sin\varphi}{R_0} + \beta_s \tag{3}$$

In the above, the first three strains $\varepsilon_x^0, \varepsilon_s^0, \gamma_{xs}^0$ are the in-plane meridional, circumferential and shearing components, $\chi_x, \chi_s, \chi_{xs}$ are the analogous curvature changes. The last two components γ_{xn}, γ_{sn} are transverse shearing strains. The matrix notation of the congruence equations assumes the aspect:

$$\boldsymbol{\varepsilon} = \mathbf{D}\mathbf{u} \tag{4}$$

where

$$\mathbf{D} = \begin{bmatrix} \frac{\partial}{\partial x} & 0 & 0 & 0 & 0 \\ \frac{\cos\varphi}{R_0} & \frac{\partial}{\partial s} & \frac{\sin\varphi}{R_0} & 0 & 0 \\ \frac{\partial}{\partial s} & \frac{\partial}{\partial x} - \frac{\cos\varphi}{R_0} & 0 & 0 & 0 \\ 0 & 0 & 0 & \frac{\partial}{\partial x} & 0 \\ 0 & 0 & 0 & \frac{\cos\varphi}{R_0} & \frac{\partial}{\partial s} \\ 0 & 0 & 0 & \frac{\partial}{\partial s} & \frac{\partial}{\partial x} - \frac{\cos\varphi}{R_0} \\ 0 & 0 & \frac{\partial}{\partial x} & 1 & 0 \\ 0 & -\frac{\sin\varphi}{R_0} & \frac{\partial}{\partial s} & 0 & 1 \end{bmatrix} \tag{5}$$

is meant to indicate the congruence operator or the kinematic operator and

$$\mathbf{u}(x,s,t) = [u_x \;\; u_s \;\; w \;\; \beta_x \;\; \beta_s]^{\mathrm{T}} \tag{6}$$

$$\boldsymbol{\varepsilon}(x,s,t) = [\varepsilon_x^0 \;\; \varepsilon_s^0 \;\; \gamma_{xs}^0 \;\; \chi_x \;\; \chi_s \;\; \chi_{xs} \;\; \gamma_{xn} \;\; \gamma_{sn}]^{\mathrm{T}} \tag{7}$$

denote the displacement vector $\mathbf{u}$ and the generalized strain vector $\boldsymbol{\varepsilon}$, respectively. The congruence operator $\mathbf{D}$ is also known as the definition operator, because Eqs. (3) in discussion are known as the definition equations too.

2.2. Constitutive equations

The shell material assumed in the following is a functionally graded linear elastic one. Accordingly, the following constitutive equations relate internal stress resultants and internal couples with generalized strain components on the middle surface:

$$\begin{bmatrix} N_x \\ N_s \\ N_{xs} \\ M_x \\ M_s \\ M_{xs} \\ T_x \\ T_s \end{bmatrix} = \begin{bmatrix} A_{11} & A_{12} & 0 & B_{11} & B_{12} & 0 & 0 & 0 \\ A_{12} & A_{11} & 0 & B_{12} & B_{11} & 0 & 0 & 0 \\ 0 & 0 & A_{66} & 0 & 0 & B_{66} & 0 & 0 \\ B_{11} & B_{12} & 0 & D_{11} & D_{12} & 0 & 0 & 0 \\ B_{12} & B_{11} & 0 & D_{12} & D_{11} & 0 & 0 & 0 \\ 0 & 0 & B_{66} & 0 & 0 & D_{66} & 0 & 0 \\ 0 & 0 & 0 & 0 & 0 & 0 & \kappa A_{66} & 0 \\ 0 & 0 & 0 & 0 & 0 & 0 & 0 & \kappa A_{66} \end{bmatrix} \begin{bmatrix} \varepsilon_x^0 \\ \varepsilon_s^0 \\ \gamma_{xs}^0 \\ \chi_x \\ \chi_s \\ \chi_{xs} \\ \gamma_{xn} \\ \gamma_{sn} \end{bmatrix} \tag{8}$$

where κ is the shear correction factor, which is usually taken as $\kappa = 5/6$. In Eq. (8), the first three components N_x, N_s, N_{xs} are the in-plane meridional, circumferential and shearing force resultants, M_x, M_s, M_{xs} are the analogous couples, while the last two T_x, T_s are the transverse shears. In matrix notation, the relation between the generalized stress resultants per unit

length and the generalized strain components takes the form:

$$\mathbf{S} = \mathbf{C}\boldsymbol{\varepsilon} \tag{9}$$

where

$$\mathbf{C} = \begin{bmatrix} A_{11} & A_{12} & 0 & B_{11} & B_{12} & 0 & 0 & 0 \\ A_{12} & A_{11} & 0 & B_{12} & B_{11} & 0 & 0 & 0 \\ 0 & 0 & A_{66} & 0 & 0 & B_{66} & 0 & 0 \\ B_{11} & B_{12} & 0 & D_{11} & D_{12} & 0 & 0 & 0 \\ B_{12} & B_{11} & 0 & D_{12} & D_{11} & 0 & 0 & 0 \\ 0 & 0 & B_{66} & 0 & 0 & D_{66} & 0 & 0 \\ 0 & 0 & 0 & 0 & 0 & 0 & \kappa A_{66} & 0 \\ 0 & 0 & 0 & 0 & 0 & 0 & 0 & \kappa A_{66} \end{bmatrix} \tag{10}$$

is the constitutive operator, also called matrix of the material rigidity and

$$\mathbf{S}(x,s,t) = [N_x \;\; N_s \;\; N_{xs} \;\; M_x \;\; M_s \;\; M_{xs} \;\; T_x \;\; T_s]^{\mathrm{T}} \tag{11}$$

is the vector of internal stress resultants also termed internal force vector. The extensional stiffnesses A_{ij}, the bending stiffnesses D_{ij} and the bending–extensional coupling stiffnesses B_{ij} are defined as

$$A_{ij} = \int_{-(h/2)}^{h/2} Q_{ij}(\zeta)\,\mathrm{d}\zeta, \quad B_{ij} = \int_{-(h/2)}^{h/2} Q_{ij}(\zeta)\zeta\,\mathrm{d}\zeta, \quad D_{ij} = \int_{-(h/2)}^{h/2} Q_{ij}(\zeta)\zeta^2\,\mathrm{d}\zeta \tag{12}$$

where the elastic constants $Q_{ij} = Q_{ij}(\zeta)$ are functions of thickness coordinate ζ and are defined as

$$Q_{11} = \frac{E(\zeta)}{1-\nu^2(\zeta)}, \quad Q_{12} = \frac{\nu(\zeta)E(\zeta)}{1-\nu^2(\zeta)}, \quad Q_{66} = \frac{E(\zeta)}{2(1+\nu(\zeta))} \tag{13}$$

It is worth noting that, due to the dependence of elastic constants $Q_{ij} = Q_{ij}(\zeta)$ (13) from the thickness coordinate ζ, in this work stiffnesses (12) are numerically computed using the *quadl* MatLab function. In fact, since closed form expressions for coefficients (12) are not easy to obtain for any kind of the material property variation through the thickness, integrals (12) are numerically evaluated using recursive adaptive Lobatto quadrature.

It is assumed that the FGM shell is made of a mixture of a ceramic and metallic constituent. The material properties of the functionally graded shell vary continuously and smoothly in the thickness direction ζ and are functions of the volume fractions and properties of the constituent materials. The Young's modulus $E(\zeta)$, Poisson's ratio $\nu(\zeta)$ and mass density $\rho(\zeta)$ of the functionally graded shell can be expressed as a linear combination:

$$\rho(\zeta) = (\rho_C - \rho_M)V_C + \rho_M, \quad E(\zeta) = (E_C - E_M)V_C + E_M, \quad \nu(\zeta) = (\nu_C - \nu_M)V_C + \nu_M \tag{14}$$

where ρ_C, E_C, ν_C, V_C and ρ_M, E_M, ν_M, V_M represent mass density, Young's modulus, Poisson's ratio and volume fraction of the ceramic and metallic constituent materials, respectively. The volume fractions of all the constituent materials should add up to unity:

$$V_C + V_M = 1 \tag{15}$$

In this paper, the ceramic volume fraction V_C follows two simple power-law distributions:

$$\mathrm{FGM}_1: \quad V_C = \left(\frac{1}{2} - \frac{\zeta}{h}\right)^p, \quad \mathrm{FGM}_2: \quad V_C = \left(\frac{1}{2} + \frac{\zeta}{h}\right)^p \tag{16}$$

where the volume fraction index p ($0 \le p \le \infty$) dictates the material variation profile through the functionally graded shell thickness. It is worth noting that, when $p = 0$ or ∞, the isotropic and homogeneous material is obtained. These material variations are illustrated in Fig. 2.

2.3. Equations of motion in terms of internal actions

Following the direct approach or the Hamilton's principle in dynamic version and remembering the Gauss–Codazzi relations for the shells of revolution considered $\mathrm{d}R_0/\mathrm{d}x = \cos\,\varphi$, five equations of dynamic equilibrium in terms of internal actions can be written for the shell element:

$$\frac{\partial N_x}{\partial x} + \frac{\partial N_{xs}}{\partial s} + (N_x - N_s)\frac{\cos\,\varphi}{R_0} + q_x = I_0\ddot{u}_x + I_1\ddot{\beta}_x$$

$$\frac{\partial N_{xs}}{\partial x} + \frac{\partial N_s}{\partial s} + 2N_{xs}\frac{\cos\,\varphi}{R_0} + T_s\frac{\sin\,\varphi}{R_0} + q_s = I_0\ddot{u}_s + I_1\ddot{\beta}_s$$

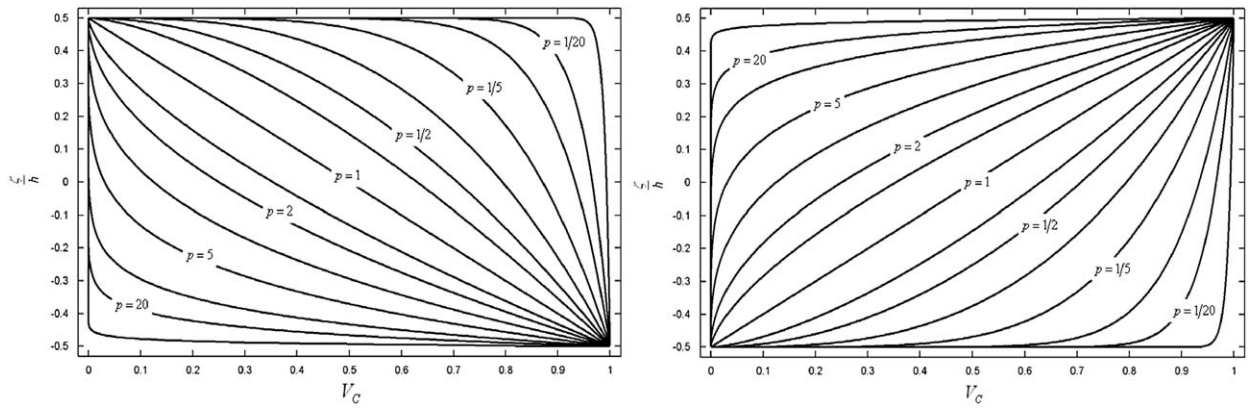

Fig. 2. Variation of the ceramic volume fraction V_C through the thickness for different values of power-law index p: (a) FGM_1 distribution and (b) FGM_2 distribution.

$$\frac{\partial T_x}{\partial x}+\frac{\partial T_s}{\partial s}+T_x\frac{\cos\varphi}{R_0}-N_s\frac{\sin\varphi}{R_0}+q_n=I_0\ddot{w}$$

$$\frac{\partial M_x}{\partial x}+\frac{\partial M_{xs}}{\partial s}+(M_x-M_s)\frac{\cos\varphi}{R_0}-T_x+m_x=I_1\ddot{u}_x+I_2\ddot{\beta}_x$$

$$\frac{\partial M_{xs}}{\partial x}+\frac{\partial M_s}{\partial s}+2M_{xs}\frac{\cos\varphi}{R_0}-T_s+m_s=I_1\ddot{u}_s+I_2\ddot{\beta}_s \tag{17}$$

where

$$I_i=\int_{-h/2}^{h/2}\rho(\zeta)\zeta^i\left(1+\frac{\zeta}{R_\vartheta}\right)\mathrm{d}\zeta,\quad i=0,1,2 \tag{18}$$

are the mass inertias. The first three equations (17) represent translational equilibriums along meridional, circumferential and normal directions, while the last two are rotational equilibrium equations about the x and s directions.

Equations of motion or dynamic equilibrium equations (17) can be written in the operatorial form:

$$\mathbf{D}^*\mathbf{S}=\mathbf{q}-\frac{\partial\mathbf{\Lambda}}{\partial t}\quad\text{or}\quad\mathbf{D}^*\mathbf{S}=\mathbf{f} \tag{19}$$

where

$$\mathbf{q}(x,s,t)=[q_x\ \ q_s\ \ q_n\ \ m_x\ \ m_s]^{\mathrm{T}} \tag{20}$$

$$\mathbf{\Lambda}(x,s,t)=\mathbf{M}\dot{\mathbf{u}} \tag{21}$$

are the distributed external load and the momentum vectors, respectively, and

$$\mathbf{M}=\begin{bmatrix}I_0 & 0 & 0 & I_1 & 0\\ 0 & I_0 & 0 & 0 & I_1\\ 0 & 0 & I_0 & 0 & 0\\ I_1 & 0 & 0 & I_2 & 0\\ 0 & I_1 & 0 & 0 & I_2\end{bmatrix} \tag{22}$$

is the mass matrix, while

$$\dot{\mathbf{u}}(x,s,t)=\frac{\partial}{\partial t}[u_x\ \ u_s\ \ w\ \ \beta_x\ \ \beta_s]^{\mathrm{T}} \tag{23}$$

is the derivative of the displacement vector $\mathbf{u}$ with respect to the variable t, that is the vector velocity.

The balance operator, also known as the equilibrium operator, assumes the aspect:

$$\mathbf{D}^{*}=-\begin{bmatrix} \frac{\cos\varphi}{R_0}+\frac{\partial}{\partial x} & -\frac{\cos\varphi}{R_0} & \frac{\partial}{\partial s} & 0 & 0 & 0 & 0 & 0 \\ 0 & \frac{\partial}{\partial s} & 2\frac{\cos\varphi}{R_0}+\frac{\partial}{\partial x} & 0 & 0 & 0 & 0 & \frac{\sin\varphi}{R_0} \\ 0 & -\frac{\sin\varphi}{R_0} & 0 & 0 & 0 & 0 & \frac{\cos\varphi}{R_0}+\frac{\partial}{\partial x} & \frac{\partial}{\partial s} \\ 0 & 0 & 0 & \frac{\cos\varphi}{R_0}+\frac{\partial}{\partial x} & -\frac{\cos\varphi}{R_0} & \frac{\partial}{\partial s} & -1 & 0 \\ 0 & 0 & 0 & 0 & \frac{\partial}{\partial s} & 2\frac{\cos\varphi}{R_0}+\frac{\partial}{\partial x} & 0 & -1 \end{bmatrix} \tag{24}$$

2.4. Fundamental equations

The three basic sets of equations, namely the kinematic, equilibrium and constitutive equations may be combined to give the fundamental system of equations, also known as the governing system equations. Firstly, the fundamental equations are deducted in the matrix notation. So, if the strain–displacement relations (4) are inserted into the constitutive equations (9), we have the relationships between stress resultants and the generalized displacement components:

$$\mathbf{S}=\mathbf{C}\boldsymbol{\varepsilon}=\mathbf{C}\mathbf{D}\mathbf{u} \tag{25}$$

When Eqs. (25) are inserted into the equations of motion (19), the fundamental system of equations is derived:

$$\mathbf{D}^{*}\mathbf{C}\mathbf{D}\mathbf{u}=\mathbf{q}-\frac{\partial\boldsymbol{\Lambda}}{\partial t} \quad \text{or} \quad \mathbf{D}^{*}\mathbf{C}\mathbf{D}\mathbf{u}=\mathbf{f} \tag{26}$$

Motion equations in terms of displacements take all the three aspects of the problem of the elastic equilibrium issue into account. By introducing the fundamental operator, also known as the elasticity operator,

$$\mathbf{L}=\mathbf{D}^{*}\mathbf{C}\mathbf{D} \tag{27}$$

Eq. (26) can be written as

$$\mathbf{L}\mathbf{u}=\mathbf{q}-\frac{\partial\boldsymbol{\Lambda}}{\partial t} \quad \text{or} \quad \mathbf{L}\mathbf{u}=\mathbf{f} \tag{28}$$

The fundamental system of equations (28) relates the configuration variable **u** to the source variable **q** of the phenomenon under investigation. We can summarize all these aspects of any problem of elastic problem of equilibrium into the scheme of the physical theories or Tonti's diagram, which assumes the aspect reported in Fig. 3.

Thus, the complete equations of motion in terms of displacements (28) can be written in the extended form as

(1) *Translational equilibrium along the meridional direction x*:

$$\begin{aligned} &\left(A_{11}\frac{\partial^2}{\partial x^2}+\frac{A_{11}\cos\varphi}{R_0}\frac{\partial}{\partial x}+A_{66}\frac{\partial^2}{\partial s^2}-\frac{A_{11}\cos^2\varphi}{R_0^2}\right)u_x+\left(-\left(\frac{A_{11}\cos\varphi}{R_0}+\frac{A_{66}\cos\varphi}{R_0}\right)\frac{\partial}{\partial s}+(A_{12}+A_{66})\frac{\partial^2}{\partial x\,\partial s}\right)u_s \\ &+\left(\frac{A_{12}\sin\varphi}{R_0}\frac{\partial}{\partial x}-\frac{A_{11}\sin\varphi\cos\varphi}{R_0^2}\right)w+\left(B_{11}\frac{\partial^2}{\partial x^2}+\frac{B_{11}\cos\varphi}{R_0}\frac{\partial}{\partial x}+B_{66}\frac{\partial^2}{\partial s^2}-\frac{B_{11}\cos^2\varphi}{R_0^2}\right)\beta_x \\ &+\left(-\left(\frac{B_{11}\cos\varphi}{R_0}+\frac{B_{66}\cos\varphi}{R_0}\right)\frac{\partial}{\partial s}+(B_{12}+B_{66})\frac{\partial^2}{\partial x\,\partial s}\right)\beta_s+q_x=I_0\ddot{u}_x+I_1\ddot{\beta}_x \end{aligned} \tag{29}$$

(2) *Translational equilibrium along the circumferential direction s*:

$$\begin{aligned} &\left(\left(\frac{A_{11}\cos\varphi}{R_0}+\frac{A_{66}\cos\varphi}{R_0}\right)\frac{\partial}{\partial s}+(A_{12}+A_{66})\frac{\partial^2}{\partial x\,\partial s}\right)u_x \\ &+\left(A_{66}\frac{\partial^2}{\partial x^2}+\frac{A_{66}\cos\varphi}{R_0}\frac{\partial}{\partial x}+A_{11}\frac{\partial^2}{\partial s^2}-\frac{A_{66}\cos^2\varphi}{R_0^2}-\kappa\frac{A_{66}\sin^2\varphi}{R_0^2}\right)u_s \\ &+\left(\frac{A_{11}\sin\varphi}{R_0}+\kappa\frac{A_{66}\sin\varphi}{R_0}\right)\frac{\partial w}{\partial s}+\left(\left(\frac{B_{11}\cos\varphi}{R_0}+\frac{B_{66}\cos\varphi}{R_0}\right)\frac{\partial}{\partial s}+(B_{12}+B_{66})\frac{\partial^2}{\partial x\,\partial s}\right)\beta_x \\ &+\left(B_{66}\frac{\partial^2}{\partial x^2}+\frac{B_{66}\cos\varphi}{R_0}\frac{\partial}{\partial x}+B_{11}\frac{\partial^2}{\partial s^2}-\frac{B_{66}\cos^2\varphi}{R_0^2}+\kappa\frac{A_{66}\sin\varphi}{R_0}\right)\beta_s+q_s=I_0\ddot{u}_s+I_1\ddot{\beta}_s \end{aligned} \tag{30}$$

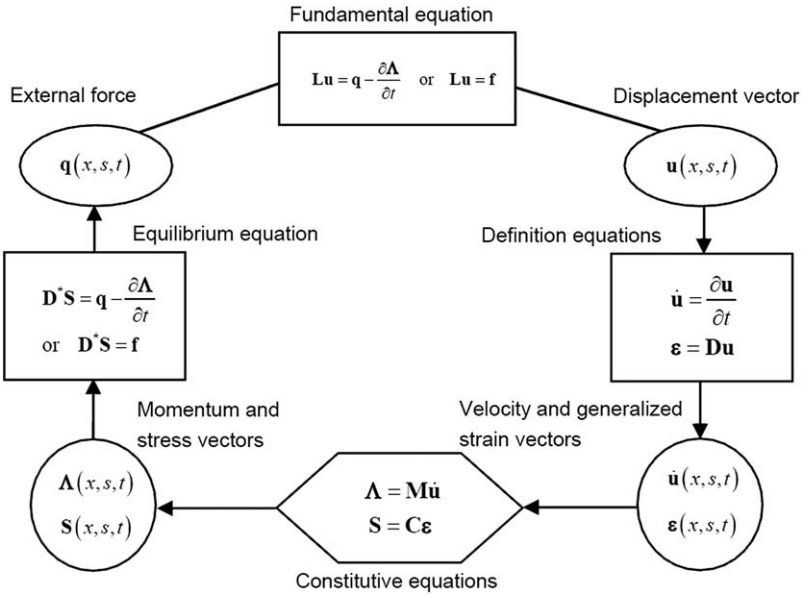

Fig. 3. Scheme of physical theories also known as Tonti's diagram.

(3) *Translational equilibrium along the normal direction* ζ:

$$\begin{aligned}&\left(-\frac{A_{12}\sin\varphi}{R_0}\frac{\partial}{\partial x}-\frac{A_{11}\sin\varphi\cos\varphi}{R_0^2}\right)u_x-\left(\frac{A_{11}\sin\varphi}{R_0}+\kappa\frac{A_{66}\sin\varphi}{R_0}\right)\frac{\partial u_s}{\partial s}\\&+\left(\kappa A_{66}\frac{\partial^2}{\partial x^2}+\kappa\frac{A_{66}\cos\varphi}{R_0}\frac{\partial}{\partial x}+\kappa A_{66}\frac{\partial^2}{\partial s^2}-\frac{A_{11}\sin^2\varphi}{R_0^2}\right)w\\&+\left(\left(-\frac{B_{12}\sin\varphi}{R_0}+\kappa A_{66}\right)\frac{\partial}{\partial x}-\frac{B_{11}\sin\varphi\cos\varphi}{R_0^2}+\kappa\frac{A_{66}\cos\varphi}{R_0}\right)\beta_x\\&+\left(-\frac{B_{11}\sin\varphi}{R_0}+\kappa A_{66}\right)\frac{\partial\beta_s}{\partial s}+q_n=I_0\ddot{w}\end{aligned}\tag{31}$$

(4) *Rotational equilibrium about the circumferential direction* s:

$$\begin{aligned}&\left(B_{11}\frac{\partial^2}{\partial x^2}+\frac{B_{11}\cos\varphi}{R_0}\frac{\partial}{\partial x}+B_{66}\frac{\partial^2}{\partial s^2}-\frac{B_{11}\cos^2\varphi}{R_0^2}\right)u_x+\left(-\left(\frac{B_{11}\cos\varphi}{R_0}+\frac{B_{66}\cos\varphi}{R_0}\right)\frac{\partial}{\partial s}+(B_{12}+B_{66})\frac{\partial^2}{\partial x\,\partial s}\right)u_s\\&+\left(\left(\frac{B_{12}\sin\varphi}{R_0}-\kappa A_{66}\right)\frac{\partial}{\partial x}-\frac{B_{11}\sin\varphi\cos\varphi}{R_0^2}\right)w+\left(D_{11}\frac{\partial^2}{\partial x^2}+\frac{D_{11}\cos\varphi}{R_0}\frac{\partial}{\partial x}+D_{66}\frac{\partial^2}{\partial s^2}-\frac{D_{11}\cos^2\varphi}{R_0^2}-\kappa A_{66}\right)\beta_x\\&+\left(-\left(\frac{D_{11}\cos\varphi}{R_0}+\frac{D_{66}\cos\varphi}{R_0}\right)\frac{\partial}{\partial s}+(D_{12}+D_{66})\frac{\partial^2}{\partial x\,\partial s}\right)\beta_s+m_x=I_1\ddot{u}_x+I_2\ddot{\beta}_x\end{aligned}\tag{32}$$

(5) *Rotational equilibrium about the meridional direction* x:

$$\begin{aligned}&\left(\left(\frac{B_{11}\cos\varphi}{R_0}+\frac{B_{66}\cos\varphi}{R_0}\right)\frac{\partial}{\partial s}+(B_{12}+B_{66})\frac{\partial^2}{\partial x\,\partial s}\right)u_x+\left(B_{66}\frac{\partial^2}{\partial x^2}+\frac{B_{66}\cos\varphi}{R_0}\frac{\partial}{\partial x}+B_{11}\frac{\partial^2}{\partial s^2}-\frac{B_{66}\cos^2\varphi}{R_0^2}+\kappa\frac{A_{66}\sin\varphi}{R_0}\right)u_s\\&+\left(\frac{B_{11}\sin\varphi}{R_0}-\kappa A_{44}\right)\frac{\partial w}{\partial s}+\left(\left(\frac{D_{11}\cos\varphi}{R_0}+\frac{D_{66}\cos\varphi}{R_0}\right)\frac{\partial}{\partial s}+(D_{12}+D_{66})\frac{\partial^2}{\partial x\,\partial s}\right)\beta_x\\&+\left(D_{66}\frac{\partial^2}{\partial x^2}+\frac{D_{66}\cos\varphi}{R_0}\frac{\partial}{\partial x}+D_{11}\frac{\partial^2}{\partial s^2}-\frac{D_{66}\cos^2\varphi}{R_0^2}-\kappa A_{66}\right)\beta_s+m_s=I_1\ddot{u}_s+I_2\ddot{\beta}_s\end{aligned}\tag{33}$$

2.5. Boundary and compatibility conditions

In the following, three kinds of boundary conditions are considered, namely the fully clamped edge boundary condition (C), the simply supported edge boundary condition (S) and the free edge boundary condition (F). The equations describing the boundary conditions can be written as follows:

Clamped edge boundary condition (*C*):

$$u_x = u_s = w = \beta_x = \beta_s = 0 \quad \text{at} \quad x = 0 \text{ or } x = x_0, \quad 0 \le s \le s_0 \tag{34}$$

$$u_x = u_s = w = \beta_x = \beta_s = 0 \quad \text{at} \quad s = 0 \text{ or } s = s_0, \quad 0 \le x \le x_0 \tag{35}$$

Simply supported edge boundary condition (*S*):

$$u_x = u_s = w = \beta_s = 0, \quad M_x = 0 \quad \text{at} \quad x = 0 \text{ or } x = x_0, \quad 0 \le s \le s_0 \tag{36}$$

$$u_x = u_s = w = \beta_x = 0, \quad M_s = 0 \quad \text{at} \quad s = 0 \text{ or } s = s_0, \quad 0 \le x \le x_0 \tag{37}$$

Free edge boundary condition (*F*):

$$N_x = N_{xs} = T_x = M_x = M_{xs} = 0 \quad \text{at} \quad x = 0 \text{ or } x = x_0, \quad 0 \le s \le s_0 \tag{38}$$

$$N_s = N_{xs} = T_s = M_s = M_{xs} = 0 \quad \text{at} \quad s = 0 \text{ or } s = s_0, \quad 0 \le x \le x_0 \tag{39}$$

In addition to the external boundary conditions, the *kinematic* and *physical compatibility* should be satisfied at the common meridian with $s = 0, 2\pi R_0$, if we want to consider a complete shell of revolution. The kinematic compatibility conditions include the continuity of displacements. The physical compatibility conditions can only be the five continuous conditions for the generalized stress resultants. To consider complete revolution conical, cylindrical shells and annular plates characterized by $s_0 = 2\pi R_0$, it is necessary to implement the kinematic and physical compatibility conditions between the two meridians with $s = 0$ and $s_0 = 2\pi R_0$:

Kinematic compatibility conditions:

$$\begin{aligned} &u_x(x,0,t) = u_x(x,s_0,t), u_s(x,0,t) = u_s(x,s_0,t), w(x,0,t) = w(x,s_0,t), \\ &\beta_x(x,0,t) = \beta_x(x,s_0,t), \beta_s(x,0,t) = \beta_s(x,s_0,t) \end{aligned} \quad 0 \le x \le x_0 \tag{40}$$

Physical compatibility conditions:

$$\begin{aligned} &N_s(x,0,t) = N_s(x,s_0,t), N_{xs}(x,0,t) = N_{xs}(x,s_0,t), T_s(x,0,t) = T_s(x,s_0,t), \\ &M_s(x,0,t) = M_s(x,s_0,t), M_{xs}(x,0,t) = M_{xs}(x,s_0,t) \end{aligned} \quad 0 \le x \le x_0 \tag{41}$$

3. Generalized differential quadrature method review

The GDQ method will be used to discretize the derivatives in the governing equations and the boundary conditions. The GDQ approach was developed by Shu [44] to improve the differential quadrature technique [45,46] for the computation of weighting coefficients, entering into the linear algebraic system of equations obtained from the discretization of the differential equation system, which can model the physical problem considered. The differential quadrature methodology has been applied in many fields of structural mechanics, as shown in the literature [38,47–51]. The essence of the differential quadrature method is that the partial derivative of a smooth function with respect to a variable is approximated by a weighted sum of function values at all discrete points in that direction. Its weighting coefficients are not related to any special problem and only depend on the grid points and the derivative order. In this methodology, an arbitrary grid distribution can be chosen without any limitation.

The GDQ method is based on the analysis of a high-order polynomial approximation and the analysis of a linear vector space [37]. For a general problem, it may not be possible to express the solution of the corresponding partial differential equation in a closed form. This solution function can be approximated by the two following types of function approximation: high-order polynomial approximation and Fourier series expansion (harmonic functions). It is well known that a smooth function in a domain can be accurately approximated by a high-order polynomial in accordance with the Weierstrass polynomial approximation theorem. In fact, from the Weierstrass theorem, if $f(x)$ is a real valued continuous function defined in the closed interval $[a, b]$, then there exists a sequence of polynomials $P_r(x)$ which converges to $f(x)$ uniformly as r goes to infinity. In practical applications, a truncated finite polynomial may be used. Thus, if $f(x)$ represents the solution of a partial differential equation, then it can be approximated by a polynomial of a degree less than or equal to $N-1$, for N large enough. The conventional form of this approximation is

$$f(x) \cong P_N(x) = \sum_{j=1}^{N} d_j p_j(x) \tag{42}$$

where d_j is a constant. Then it is easy to show that the polynomial $P_N(x)$ constitutes an N-dimensional linear vector space V_N with respect to the operation of vector addition and scalar multiplication. Obviously, in the linear vector space V_N, $p_j(x)$ is a set of base vectors. It can be seen that, in the linear polynomial vector space, there exist several sets of base polynomials and each set of base polynomials can be expressed uniquely by another set of base polynomials in the space. Using vector space analysis, the method for computing the weighting coefficients can be generalized by a proper choice of base polynomials in a linear vector space. For generality, the Lagrange interpolation polynomials are chosen as the base polynomials. As a result, the weighting coefficients of the first-order derivative are computed by a simple algebraic formulation without any restriction on the choice of the grid points, while the weighting coefficients of the second and higher order derivatives are given by a recurrence relationship.

When the Lagrange interpolated polynomials are assumed as a set of vector space base functions, the approximation of the function $f(x)$ can be written as

$$f(x) \cong \sum_{j=1}^{N} p_j(x) f(x_j) \tag{43}$$

where N is the number of grid points in the whole domain, x_j, $j = 1, 2, \ldots, N$, are the coordinates of grid points in the variable domain and $f(x_j)$ are the function values at the grid points. $p_j(x)$ are the Lagrange interpolated polynomials, which can be defined by the following formula:

$$p_j(x) = \frac{\mathsf{L}(x)}{(x - x_j)\mathsf{L}^{(1)}(x_j)}, \quad j = 1, 2, \ldots, N \tag{44}$$

where

$$\mathsf{L}(x) = \prod_{i=1}^{N} (x - x_i), \quad \mathsf{L}^{(1)}(x_j) = \prod_{i=1, i \neq j}^{N} (x_j - x_i) \tag{45}$$

Differentiating Eq. (43) with respect to x and evaluating the first derivative at a certain point of the function domain, it is possible to obtain:

$$f^{(1)}(x_i) \cong \sum_{j=1}^{N} p_j^{(1)}(x_i) f(x_j) = \sum_{j=1}^{N} \varsigma_{ij}^{(1)} f(x_j), \quad i = 1, 2, \ldots, N \tag{46}$$

where $\varsigma_{ij}^{(1)}$ are the GDQ weighting coefficients of the first-order derivative and x_i denote the coordinates of the grid points. In particular, it is worth noting that the weighting coefficients of the first-order derivative can be computed as

$$p_j^{(1)}(x_i) = \varsigma_{ij}^{(1)} = \frac{\mathsf{L}^{(1)}(x_i)}{(x_i - x_j)\mathsf{L}^{(1)}(x_j)}, \quad i, j = 1, 2, \ldots, N, \ i \neq j \tag{47}$$

From Eq. (47), $\varsigma_{ij}^{(1)}$ $(i \neq j)$ can be easily computed. However, the calculation of $\varsigma_{ii}^{(1)}$ is not easy to compute. According to the analysis of a linear vector space, one set of base functions can be expressed uniquely by a linear sum of another set of base functions. Thus, if one set of base polynomials satisfy a linear equation like (46), so does another set of base polynomials. As a consequence, the equation system for determining $\varsigma_{ij}^{(1)}$ and derived from the Lagrange interpolation polynomials should be equivalent to that derived from another set of base polynomials, i.e. $p_j(x) = x^{j-1}$, $j = 1, 2, \ldots, N$. Thus, $\varsigma_{ij}^{(1)}$ satisfies the following equation, which is obtained by the base polynomials $p_j(x) = x^{j-1}$, when $j = 1$:

$$\sum_{j=1}^{N} \varsigma_{ij}^{(1)} = 0 \ \Rightarrow \ \varsigma_{ii}^{(1)} = -\sum_{j=1, j \neq i}^{N} \varsigma_{ij}^{(1)}, \quad i, j = 1, 2, \ldots, N \tag{48}$$

Eqs. (47) and (48) are two formulations to compute the weighting coefficients $\varsigma_{ij}^{(1)}$. It should be noted that, in the development of these formulations, two sets of base polynomials were used in the linear polynomial vector space V_N. Finally, the n-th order derivative of function $f(x)$ with respect to x at grid points x_i, can be approximated by the GDQ approach:

$$\left.\frac{d^n f(x)}{dx^n}\right|_{x=x_i} = \sum_{j=1}^{N} \varsigma_{ij}^{(n)} f(x_j), \qquad i = 1, 2, \ldots, N \tag{49}$$

where $\varsigma_{ij}^{(n)}$ are the weighting coefficients of the n-th order derivative. Similar to the first-order derivative and according to the polynomial approximation and the analysis of a linear vector space, it is possible to determine a recurrence relationship to compute the second and higher order derivatives. Thus, the weighting coefficients can be generated by the following

recurrent formulation:

$$\varsigma_{ij}^{(n)} = n\left(\varsigma_{ii}^{(n-1)}\varsigma_{ij}^{(1)} - \frac{\varsigma_{ij}^{(n-1)}}{x_i - x_j}\right), \quad i \neq j, \;\; n = 2,3,\ldots,N-1, \;\; i,j = 1,2,\ldots,N \tag{50}$$

$$\sum_{j=1}^{N} \varsigma_{ij}^{(n)} = 0 \;\Rightarrow\; \varsigma_{ii}^{(n)} = -\sum_{j=1, j\neq i}^{N} \varsigma_{ij}^{(n)}, \quad n = 2,3,\ldots,N-1, \;\; i,j = 1,2,\ldots,N \tag{51}$$

It is obvious from the above equations that the weighting coefficients of the second and higher order derivatives can be determined from those of the first-order derivative. Furthermore, it is interesting to note that, the preceding coefficients $\varsigma_{ij}^{(n)}$ are dependent on the derivative order n, on the grid point distribution x_j, $j = 1,2,\ldots,N$, and on the specific point x_i, where the derivative is computed. There is no need to obtain the weighting coefficients from a set of algebraic equations which could be ill-conditioned when the number of grid points is large. The merit of the explicit formulae (47), (48), (50) and (51) is that highly accurate weighting coefficients may be determined for any number of arbitrarily spaced sampling points. Furthermore, this set of expressions for the determination of the weighting coefficients is so compact and simple that it is very easy to implement them in formulating and programming, because of the recurrence feature.

3.1. Grid distributions

Another important point for successful application of the GDQ method is how to distribute the grid points. The grid point distribution also plays an essential role in determining the accuracy, the convergence speed and the stability of the GDQ method. In this paper, the effects of the grid point distribution will be investigated for the vibration analysis of conical, cylindrical shells and annular plates. The natural and simplest choice of the grid points through the computational domain is the one having equally spaced points in the coordinate direction of the computational domain. However, it is demonstrated that non-uniform grid distribution usually yields better results than equally spaced distribution. Quan and Chang [52,53] compared numerically the performances of the often-used non-uniform meshes and concluded that the grid points originating from the Chebyshev polynomials of the first kind are optimum in all the cases examined there. The zeros of orthogonal polynomials are the rational basis for the grid points. Shu [44] used a choice which gives better results than the zeros of Chebyshev and Legendre polynomials. Bert and Malik [38] indicated that the preferred type of grid points changes with problems of interest and recommended the use of Chebyshev–Gauss–Lobatto grid for the structural mechanics computation. With Lagrange interpolating polynomials, the rule of Chebyshev–Gauss–Lobatto (C–G–L) sampling points proves efficient for numerical reasons [54] and for such a collocation the approximation error of the dependent variables decreases as the number of nodes increases. In this study, different grid point distributions are considered to investigate their effect on the GDQ solution accuracy, convergence speed and stability.

The typical distributions of grid points, which are commonly used in the literature, in normalized form are reported as follows:

Equally spaced or uniform distribution (*Uni*)

$$r_i = \frac{i-1}{N-1}, \quad i = 1,2,\ldots,N \tag{52}$$

Roots of Chebyshev polynomials of the first kind (*C* I°)

$$r_i = \frac{g_i - g_1}{g_N - g_1}, \quad g_i = \cos\left(\left(\frac{2i-1}{2N}\right)\pi\right), \quad i = 1,2,\ldots,N \tag{53}$$

Roots of Chebyshev polynomials of the second kind (*C* II°)

$$r_i = \frac{g_i - g_1}{g_N - g_1}, \quad g_i = \cos\left(\frac{i\pi}{N+1}\right), \quad i = 1,2,\ldots,N \tag{54}$$

Roots of Legendre polynomials (*Leg*)

$$r_i = \frac{g_i - g_1}{g_N - g_1}, \quad g_i = \left(1 - \frac{1}{8N^2} + \frac{1}{8N^3}\right)\cos\left(\frac{4i-1}{4N+2}\pi\right), \quad i = 1,2,\ldots,N \tag{55}$$

Quadratic sampling points distribution (*Quad*)

$$r_i = \begin{cases} 2\left(\dfrac{i-1}{N-1}\right)^2 & i = 1,2,\ldots,\dfrac{N+1}{2} \\ \left(-2\left(\dfrac{i-1}{N-1}\right)^2 + 4\left(\dfrac{i-1}{N-1}\right) - 1\right) & i = \left(\dfrac{N+1}{2}\right)+1,\ldots,N \end{cases} \tag{56}$$

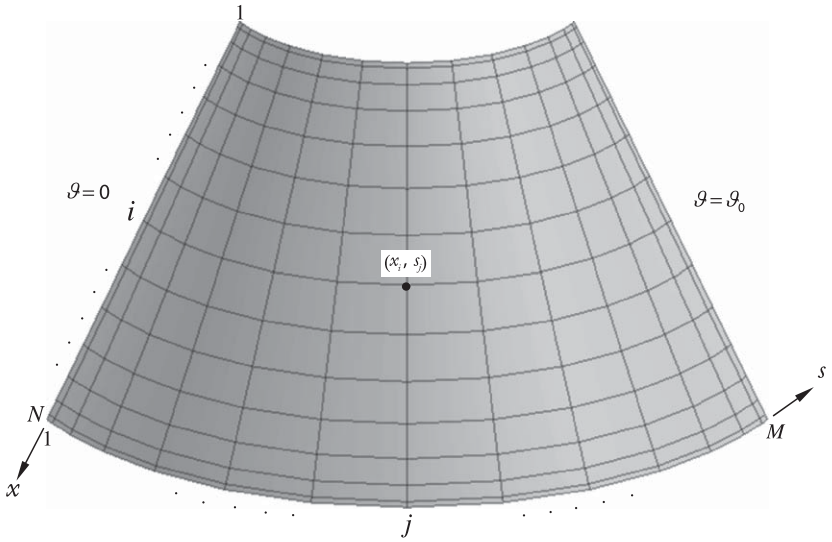

Fig. 4. C–G–L grid distribution on a conical panel.

Chebyshev–Gauss–Lobatto sampling points (*C–G–L*)

$$r_i = \frac{1 - \cos\left(\dfrac{i-1}{N-1}\right)\pi}{2}, \quad i = 1, 2, \ldots, N \tag{57}$$

where N is the total number of sampling points used to discretize each direction.

For the numerical computations presented in this paper, the coordinates of grid points (x_i, s_j) are chosen as

$$\begin{aligned} x_i &= r_i x_0, \quad i = 1, 2, \ldots, N, \ \text{ for } x \in [0, x_0] \\ s_j &= r_j s_0, \quad j = 1, 2, \ldots, M, \ \text{ for } s \in [0, s_0] \end{aligned} \tag{58}$$

where r_i, r_j are two grid distributions of previous ones and N, M are the total number of sampling points used to discretize the domain in x and s directions, respectively, of the considered shells (Fig. 4).

4. Numerical implementation

In the following, the free vibration of conical, cylindrical shells and annular plates will be studied. In solving the governing Eqs. (29)–(33), the generalized differential quadrature method is used. This method demonstrates its numerical accuracy and extreme coding simplicity. So, setting $\mathbf{q}(x, s, t) = \mathbf{0}$ and using the method of variable separation, it is possible to seek solutions that are harmonic in time and whose frequency is ω; then, the displacements and the rotations can be written as follows:

$$\begin{aligned} u_x(x, s, t) &= U^x(x, s)\, \mathrm{e}^{\mathrm{i}\omega t} \\ u_s(x, s, t) &= U^s(x, s)\, \mathrm{e}^{\mathrm{i}\omega t} \\ w(x, s, t) &= W(x, s)\, \mathrm{e}^{\mathrm{i}\omega t} \\ \beta_x(x, s, t) &= B^x(x, s)\, \mathrm{e}^{\mathrm{i}\omega t} \\ \beta_s(x, s, t) &= B^s(x, s)\, \mathrm{e}^{\mathrm{i}\omega t} \end{aligned} \tag{59}$$

where the vibration spatial amplitude values ($U^x(x, s)$, $U^s(x, s)$, $W(x, s)$, $B^x(x, s)$, $B^s(x, s)$) fulfill the fundamental differential system. The basic steps in the GDQ solution of the free vibration problem of shell type structures are as in the following:

- Discretization of independent variables $x \in [0, x_0]$, $s \in [0, s_0]$ (with $x_0 > 0$ and $s_0 \leq 2\pi R_0$).
- Approximation of the spatial derivatives according to GDQ rule.

- Transformation of the differential governing systems (29), (30), (31), (32), and (33) into linear eigenvalue problems for the natural frequencies. The boundary and compatibility conditions are imposed in the sampling points corresponding to the boundary. All these relations are imposed point-wise. These resulting equations constitute a well-posed eigenvalue problem where the number of equations is identical to the number of unknowns.
- Solution of the previously stated discrete system in terms of natural frequencies and mode shape components. For each mode, local values of dependent variables are used to obtain the complete assessment of the deformed configuration.

4.1. Discretization of motion equations

The GDQ procedure enable one to write the equations of motion in discrete form, transforming each space derivative into a weighted sum of node values of dependent variables. Each approximate equation is valid in a single sampling point. The governing equations can be discretized as

(1) *Translational equilibrium along the meridional direction x*:

$$\begin{aligned}
&A_{11}\sum_{k=1}^{N}\varsigma_{ik}^{x(2)}U_{kj}^{x}+\frac{A_{11}\cos\varphi_i}{R_{0i}}\sum_{k=1}^{N}\varsigma_{ik}^{x(1)}U_{kj}^{x}+A_{66}\sum_{m=1}^{M}\varsigma_{jm}^{s(2)}U_{im}^{x}-\frac{A_{11}\cos^2\varphi_i}{R_{0i}^2}U_{ij}^{x}\\
&-\left(\frac{A_{11}\cos\varphi_i}{R_{0i}}+\frac{A_{66}\cos\varphi_i}{R_{0i}}\right)\sum_{m=1}^{M}\varsigma_{jm}^{s(1)}U_{im}^{s}+(A_{12}+A_{66})\sum_{k=1}^{N}\varsigma_{ik}^{x(1)}\sum_{m=1}^{M}\varsigma_{jm}^{s(1)}U_{km}^{s}\\
&+\frac{A_{12}\sin\varphi_i}{R_{0i}}\sum_{k=1}^{N}\varsigma_{ik}^{x(1)}W_{kj}-\frac{A_{11}\sin\varphi_i\cos\varphi_i}{R_{0i}^2}W_{ij}+B_{11}\sum_{k=1}^{N}\varsigma_{ik}^{x(2)}B_{kj}^{x}+\frac{B_{11}\cos\varphi_i}{R_{0i}}\sum_{k=1}^{N}\varsigma_{ik}^{x(1)}B_{kj}^{x}\\
&+B_{66}\sum_{m=1}^{M}\varsigma_{jm}^{s(2)}B_{im}^{x}-\frac{B_{11}\cos^2\varphi_i}{R_{0i}^2}B_{ij}^{x}-\left(\frac{B_{11}\cos\varphi_i}{R_{0i}}+\frac{B_{66}\cos\varphi_i}{R_{0i}}\right)\sum_{m=1}^{M}\varsigma_{jm}^{s(1)}B_{im}^{s}\\
&+(B_{12}+B_{66})\sum_{k=1}^{N}\varsigma_{ik}^{x(1)}\sum_{m=1}^{M}\varsigma_{jm}^{s(1)}B_{km}^{s}=-\omega^2(I_0U_{ij}^{x}+I_1B_{ij}^{x})
\end{aligned}\tag{60}$$

(2) *Translational equilibrium along the circumferential direction s*:

$$\begin{aligned}
&\left(\frac{A_{11}\cos\varphi_i}{R_{0i}}+\frac{A_{66}\cos\varphi_i}{R_{0i}}\right)\sum_{m=1}^{M}\varsigma_{jm}^{s(1)}U_{im}^{x}+(A_{12}+A_{66})\sum_{k=1}^{N}\varsigma_{ik}^{x(1)}\sum_{m=1}^{M}\varsigma_{jm}^{s(1)}U_{km}^{x}+A_{66}\sum_{k=1}^{N}\varsigma_{ik}^{x(2)}U_{kj}^{s}\\
&+\frac{A_{66}\cos\varphi_i}{R_{0i}}\sum_{k=1}^{N}\varsigma_{ik}^{x(1)}U_{kj}^{s}+A_{11}\sum_{m=1}^{M}\varsigma_{jm}^{s(2)}U_{im}^{s}-\left(\frac{A_{66}\cos^2\varphi_i}{R_{0i}^2}+\kappa\frac{A_{66}\sin^2\varphi_i}{R_{0i}^2}\right)U_{ij}^{s}\\
&+\left(\frac{A_{11}\sin\varphi_i}{R_{0i}}+\kappa\frac{A_{66}\sin\varphi_i}{R_{0i}}\right)\sum_{m=1}^{M}\varsigma_{jm}^{s(1)}W_{im}+\left(\frac{B_{11}\cos\varphi_i}{R_{0i}}+\frac{B_{66}\cos\varphi_i}{R_{0i}}\right)\sum_{m=1}^{M}\varsigma_{jm}^{s(1)}B_{im}^{x}\\
&+(B_{12}+B_{66})\sum_{k=1}^{N}\varsigma_{ik}^{x(1)}\sum_{m=1}^{M}\varsigma_{jm}^{s(1)}B_{km}^{x}+B_{66}\sum_{k=1}^{N}\varsigma_{ik}^{x(2)}B_{kj}^{s}+\frac{B_{66}\cos\varphi_i}{R_{0i}}\sum_{k=1}^{N}\varsigma_{ik}^{x(1)}B_{kj}^{s}\\
&+B_{11}\sum_{m=1}^{M}\varsigma_{jm}^{s(2)}B_{im}^{s}-\left(\frac{B_{66}\cos^2\varphi_i}{R_{0i}^2}-\kappa\frac{A_{66}\sin\varphi_i}{R_{0i}}\right)B_{ij}^{s}=-\omega^2(I_0U_{ij}^{s}+I_1B_{ij}^{s})
\end{aligned}\tag{61}$$

(3) *Translational equilibrium along the normal direction ζ*:

$$\begin{aligned}
&-\frac{A_{12}\sin\varphi_i}{R_{0i}}\sum_{k=1}^{N}\varsigma_{ik}^{x(1)}U_{kj}^{x}-\frac{A_{11}\sin\varphi_i\cos\varphi_i}{R_{0i}^2}U_{ij}^{x}-\left(\frac{A_{11}\sin\varphi_i}{R_{0i}}+\kappa\frac{A_{66}\sin\varphi_i}{R_{0i}}\right)\sum_{m=1}^{M}\varsigma_{jm}^{s(1)}U_{im}^{s}\\
&+\kappa A_{66}\sum_{k=1}^{N}\varsigma_{ik}^{x(2)}W_{kj}+\kappa\frac{A_{66}\cos\varphi_i}{R_{0i}}\sum_{k=1}^{N}\varsigma_{ik}^{x(1)}W_{kj}+\kappa A_{66}\sum_{m=1}^{M}\varsigma_{jm}^{s(2)}W_{im}-\frac{A_{11}\sin^2\varphi_i}{R_{0i}^2}W_{ij}\\
&-\left(\frac{B_{12}\sin\varphi_i}{R_{0i}}-\kappa A_{66}\right)\sum_{k=1}^{N}\varsigma_{ik}^{x(1)}B_{kj}^{x}-\left(\frac{B_{11}\sin\varphi_i\cos\varphi_i}{R_{0i}^2}-\kappa\frac{A_{66}\cos\varphi_i}{R_{0i}}\right)B_{ij}^{x}\\
&-\left(\frac{B_{11}\sin\varphi_i}{R_{0i}}-\kappa A_{66}\right)\sum_{m=1}^{M}\varsigma_{jm}^{s(1)}B_{im}^{s}=-\omega^2I_0W_{ij}
\end{aligned}\tag{62}$$

(4) *Rotational equilibrium about the circumferential direction s*:

$$
\begin{aligned}
&B_{11}\sum_{k=1}^{N}\varsigma_{ik}^{x(2)}U_{kj}^{x}+\frac{B_{11}\cos\varphi_i}{R_{0i}}\sum_{k=1}^{N}\varsigma_{ik}^{x(1)}U_{kj}^{x}+B_{66}\sum_{m=1}^{M}\varsigma_{jm}^{s(2)}U_{im}^{x}-\frac{B_{11}\cos^2\varphi_i}{R_{0i}^2}U_{ij}^{x}\\
&-\left(\frac{B_{11}\cos\varphi_i}{R_{0i}}+\frac{B_{66}\cos\varphi_i}{R_{0i}}\right)\sum_{m=1}^{M}\varsigma_{jm}^{s(1)}U_{im}^{s}+(B_{12}+B_{66})\sum_{k=1}^{N}\varsigma_{ik}^{x(1)}\sum_{m=1}^{M}\varsigma_{jm}^{s(1)}U_{km}^{s}\\
&+\left(\frac{B_{12}\sin\varphi_i}{R_{0i}}-\kappa A_{66}\right)\sum_{k=1}^{N}\varsigma_{ik}^{x(1)}W_{kj}-\frac{B_{11}\sin\varphi_i\cos\varphi_i}{R_{0i}^2}W_{ij}+D_{11}\sum_{k=1}^{N}\varsigma_{ik}^{x(2)}B_{kj}^{x}\\
&+\frac{D_{11}\cos\varphi_i}{R_{0i}}\sum_{k=1}^{N}\varsigma_{ik}^{x(1)}B_{kj}^{x}+D_{66}\sum_{m=1}^{M}\varsigma_{jm}^{s(2)}B_{im}^{x}-\left(\frac{D_{11}\cos^2\varphi_i}{R_{0i}^2}+\kappa A_{66}\right)B_{ij}^{x}\\
&-\left(\frac{D_{11}\cos\varphi_i}{R_{0i}}+\frac{D_{66}\cos\varphi_i}{R_{0i}}\right)\sum_{m=1}^{M}\varsigma_{jm}^{s(1)}B_{im}^{s}+(D_{12}+D_{66})\sum_{k=1}^{N}\varsigma_{ik}^{x(1)}\sum_{m=1}^{M}\varsigma_{jm}^{s(1)}B_{km}^{s}\\
&=-\omega^2(I_1U_{ij}^{x}+I_2B_{ij}^{x})
\end{aligned}
\tag{63}
$$

(5) *Rotational equilibrium about the meridional direction x*:

$$
\begin{aligned}
&\left(\frac{B_{11}\cos\varphi_i}{R_{0i}}+\frac{B_{66}\cos\varphi_i}{R_{0i}}\right)\sum_{m=1}^{M}\varsigma_{jm}^{s(1)}U_{im}^{x}+(B_{12}+B_{66})\sum_{k=1}^{N}\varsigma_{ik}^{x(1)}\sum_{m=1}^{M}\varsigma_{jm}^{s(1)}U_{km}^{x}+B_{66}\sum_{k=1}^{N}\varsigma_{ik}^{x(2)}U_{kj}^{s}\\
&+\frac{B_{66}\cos\varphi_i}{R_{0i}}\sum_{k=1}^{N}\varsigma_{ik}^{x(1)}U_{kj}^{s}+B_{11}\sum_{m=1}^{M}\varsigma_{jm}^{s(2)}U_{im}^{s}-\left(\frac{B_{66}\cos^2\varphi_i}{R_{0i}^2}-\kappa\frac{A_{66}\sin\varphi_i}{R_{0i}}\right)U_{ij}^{s}\\
&+\left(\frac{B_{11}\sin\varphi_i}{R_{0i}}-\kappa A_{66}\right)\sum_{m=1}^{M}\varsigma_{jm}^{s(1)}W_{im}+\left(\frac{D_{11}\cos\varphi_i}{R_{0i}}+\frac{D_{66}\cos\varphi_i}{R_{0i}}\right)\sum_{m=1}^{M}\varsigma_{jm}^{s(1)}B_{im}^{x}\\
&+(D_{12}+D_{66})\sum_{k=1}^{N}\varsigma_{ik}^{x(1)}\sum_{m=1}^{M}\varsigma_{jm}^{s(1)}B_{km}^{x}+D_{66}\sum_{k=1}^{N}\varsigma_{ik}^{x(2)}B_{kj}^{s}+\frac{D_{66}\cos\varphi_i}{R_{0i}}\sum_{k=1}^{N}\varsigma_{ik}^{x(1)}B_{kj}^{s}\\
&+D_{11}\sum_{m=1}^{M}\varsigma_{jm}^{s(2)}B_{im}^{s}-\left(\frac{D_{66}\cos^2\varphi_i}{R_{0i}^2}+\kappa A_{66}\right)B_{ij}^{s}=-\omega^2(I_1U_{ij}^{s}+I_2B_{ij}^{s})
\end{aligned}
\tag{64}
$$

where $i=2,3,\ldots,N-1$, $j=2,3,\ldots,M-1$ and $\varsigma_{ik}^{x(1)}$, $\varsigma_{jm}^{s(1)}$, $\varsigma_{ik}^{x(2)}$ and $\varsigma_{jm}^{s(2)}$ are the weighting coefficients of the first and second derivatives in x and s directions, respectively. Furthermore, N and M are the total number of grid points in x and s directions.

4.2. Implementation of boundary and compatibility conditions

Applying the GDQ methodology, the discretized forms of the boundary and compatibility conditions are given as follows:

Clamped edge boundary condition (C):

$$
\begin{aligned}
&U_{aj}^{x}=U_{aj}^{s}=W_{aj}=B_{aj}^{x}=B_{aj}^{s}=0\quad\text{for } a=1,\ N \text{ and } j=1,2,\ldots,M\\
&U_{ib}^{x}=U_{ib}^{s}=W_{ib}=B_{ib}^{x}=B_{ib}^{s}=0\quad\text{for } b=1,\ M \text{ and } i=1,2,\ldots,N
\end{aligned}
\tag{65}
$$

Simply supported edge boundary condition (S):

$$
\begin{cases}
U_{aj}^{x}=U_{aj}^{s}=W_{aj}=B_{aj}^{s}=0\\
B_{11}\sum\limits_{k=1}^{N}\varsigma_{ak}^{x(1)}U_{kj}^{x}+\dfrac{B_{12}\cos\varphi_a}{R_{0a}}U_{aj}^{x}+B_{12}\sum\limits_{m=1}^{M}\varsigma_{jm}^{s(1)}U_{am}^{s}+\dfrac{B_{12}\sin\varphi_a}{R_{0a}}W_{aj}\quad\text{for } a=1,\ N \text{ and } j=1,2,\ldots,M\\
\quad+D_{11}\sum\limits_{k=1}^{N}\varsigma_{ak}^{x(1)}B_{kj}^{x}+\dfrac{D_{12}\cos\varphi_a}{R_{0a}}B_{aj}^{x}+D_{12}\sum\limits_{m=1}^{M}\varsigma_{jm}^{s(1)}B_{am}^{s}=0
\end{cases}
$$

$$\begin{cases} U_{ib}^{x} = U_{ib}^{s} = W_{ib} = B_{ib}^{x} = 0 \\ B_{12}\sum_{k=1}^{N}\varsigma_{ik}^{x(1)}U_{kb}^{x} + \dfrac{B_{11}\cos\varphi_i}{R_{0i}}U_{ib}^{x} + B_{11}\sum_{m=1}^{M}\varsigma_{bm}^{s(1)}U_{im}^{s} + \dfrac{B_{11}\sin\varphi_i}{R_{0i}}W_{ib} \quad \text{for } b=1,\ M \text{ and } i=1,2,\ldots,N \\ \quad +D_{12}\sum_{k=1}^{N}\varsigma_{ik}^{x(1)}B_{kb}^{x} + \dfrac{D_{11}\cos\varphi_i}{R_{0i}}B_{ib}^{x} + D_{11}\sum_{m=1}^{M}\varsigma_{bm}^{s(1)}B_{im}^{s} = 0 \end{cases} \tag{66}$$

Free edge boundary condition (F):

$$\begin{cases} A_{11}\sum_{k=1}^{N}\varsigma_{ak}^{x(1)}U_{kj}^{x} + \dfrac{A_{12}\cos\varphi_a}{R_{0a}}U_{aj}^{x} + A_{12}\sum_{m=1}^{M}\varsigma_{jm}^{s(1)}U_{am}^{s} + \dfrac{A_{12}\sin\varphi_a}{R_{0a}}W_{aj} \\ \quad +B_{11}\sum_{k=1}^{N}\varsigma_{ak}^{x(1)}B_{kj}^{x} + \dfrac{B_{12}\cos\varphi_a}{R_{0a}}B_{aj}^{x} + B_{12}\sum_{m=1}^{M}\varsigma_{jm}^{s(1)}B_{am}^{s} = 0 \\ A_{66}\sum_{m=1}^{M}\varsigma_{jm}^{s(1)}U_{am}^{x} + A_{66}\sum_{k=1}^{N}\varsigma_{ak}^{x(1)}U_{kj}^{s} - \dfrac{A_{66}\cos\varphi_a}{R_{0a}}U_{aj}^{s} \\ \quad +B_{66}\sum_{m=1}^{M}\varsigma_{jm}^{s(1)}B_{am}^{x} + B_{66}\sum_{k=1}^{N}\varsigma_{ak}^{x(1)}B_{kj}^{s} - \dfrac{B_{66}\cos\varphi_a}{R_{0a}}B_{aj}^{s} = 0 \\ \kappa A_{66}\sum_{k=1}^{N}\varsigma_{ak}^{x(1)}W_{kj} + \kappa A_{66}B_{aj}^{x} + \kappa A_{66}B_{aj}^{s} = 0 \\ B_{11}\sum_{k=1}^{N}\varsigma_{ak}^{x(1)}U_{kj}^{x} + \dfrac{B_{12}\cos\varphi_a}{R_{0a}}U_{aj}^{x} + B_{12}\sum_{m=1}^{M}\varsigma_{jm}^{s(1)}U_{am}^{s} + \dfrac{B_{12}\sin\varphi_a}{R_{0a}}W_{aj} \\ \quad +D_{11}\sum_{k=1}^{N}\varsigma_{ak}^{x(1)}B_{kj}^{x} + \dfrac{D_{12}\cos\varphi_a}{R_{0a}}B_{aj}^{x} + D_{12}\sum_{m=1}^{M}\varsigma_{jm}^{s(1)}B_{am}^{s} = 0 \\ B_{66}\sum_{m=1}^{M}\varsigma_{jm}^{s(1)}U_{am}^{x} + B_{66}\sum_{k=1}^{N}\varsigma_{ak}^{x(1)}U_{kj}^{s} - \dfrac{B_{66}\cos\varphi_a}{R_{0a}}U_{aj}^{s} \\ \quad +D_{66}\sum_{m=1}^{M}\varsigma_{jm}^{s(1)}B_{am}^{x} + D_{66}\sum_{k=1}^{N}\varsigma_{ak}^{x(1)}B_{kj}^{s} - \dfrac{D_{66}\cos\varphi_a}{R_{0a}}B_{aj}^{s} = 0 \quad \text{for } a=1,\ N \text{ and } j=1,2,\ldots,M \end{cases} \tag{67}$$

$$\begin{cases} A_{66}\sum_{m=1}^{M}\varsigma_{bm}^{s(1)}U_{im}^{x} + A_{66}\sum_{k=1}^{N}\varsigma_{ik}^{x(1)}U_{kb}^{s} - \dfrac{A_{66}\cos\varphi_i}{R_{0i}}U_{ib}^{s} \\ \quad +B_{66}\sum_{m=1}^{M}\varsigma_{bm}^{s(1)}B_{im}^{x} + B_{66}\sum_{k=1}^{N}\varsigma_{ik}^{x(1)}B_{kb}^{s} - \dfrac{B_{66}\cos\varphi_i}{R_{0i}}B_{ib}^{s} = 0 \\ A_{12}\sum_{k=1}^{N}\varsigma_{ik}^{x(1)}U_{kb}^{x} + \dfrac{A_{11}\cos\varphi_i}{R_{0i}}U_{ib}^{x} + A_{11}\sum_{m=1}^{M}\varsigma_{bm}^{s(1)}U_{im}^{s} + \dfrac{A_{11}\sin\varphi_i}{R_{0i}}W_{ib} \\ \quad +B_{12}\sum_{k=1}^{N}\varsigma_{ik}^{x(1)}B_{kb}^{x} + \dfrac{B_{11}\cos\varphi_i}{R_{0i}}B_{ib}^{x} + B_{11}\sum_{m=1}^{M}\varsigma_{bm}^{s(1)}B_{im}^{s} = 0 \\ \kappa A_{66}\sum_{k=1}^{N}\varsigma_{ik}^{x(1)}W_{kb} + \kappa A_{66}B_{ib}^{x} + \kappa A_{66}B_{ib}^{s} = 0 \\ B_{66}\sum_{m=1}^{M}\varsigma_{bm}^{s(1)}U_{im}^{x} + B_{66}\sum_{k=1}^{N}\varsigma_{ik}^{x(1)}U_{kb}^{s} - \dfrac{B_{66}\cos\varphi_i}{R_{0i}}U_{ib}^{s} \\ \quad +D_{66}\sum_{m=1}^{M}\varsigma_{bm}^{s(1)}B_{im}^{x} + D_{66}\sum_{k=1}^{N}\varsigma_{ik}^{x(1)}B_{kb}^{s} - \dfrac{D_{66}\cos\varphi_i}{R_{0i}}B_{ib}^{s} = 0 \\ B_{12}\sum_{k=1}^{N}\varsigma_{ik}^{x(1)}U_{kb}^{x} + \dfrac{B_{11}\cos\varphi_i}{R_{0i}}U_{ib}^{x} + B_{11}\sum_{m=1}^{M}\varsigma_{bm}^{s(1)}U_{im}^{s} + \dfrac{B_{11}\sin\varphi_i}{R_{0i}}W_{ib} \\ \quad +D_{12}\sum_{k=1}^{N}\varsigma_{ik}^{x(1)}B_{kb}^{x} + \dfrac{D_{11}\cos\varphi_i}{R_{0i}}B_{ib}^{x} + D_{11}\sum_{m=1}^{M}\varsigma_{bm}^{s(1)}B_{im}^{s} = 0 \quad \text{for } b=1,\ M \text{ and } i=1,2,\ldots,N \end{cases} \tag{68}$$

Kinematic and physical compatibility conditions:

$$U_{i1}^{x} = U_{iM}^{x}, \quad U_{i1}^{s} = U_{iM}^{s}, \quad W_{i1} = W_{iM}, \quad B_{i1}^{x} = B_{iM}^{x}, \quad B_{i1}^{s} = B_{iM}^{s}$$

$$
\begin{cases}
A_{66}\sum_{m=1}^{M}\varsigma_{1m}^{s(1)}U_{im}^{x}+A_{66}\sum_{k=1}^{N}\varsigma_{ik}^{x(1)}U_{k1}^{s}-\dfrac{A_{66}\cos\varphi_i}{R_{0i}}U_{i1}^{s}\\
\quad+B_{66}\sum_{m=1}^{M}\varsigma_{1m}^{s(1)}B_{im}^{x}+B_{66}\sum_{k=1}^{N}\varsigma_{ik}^{x(1)}B_{k1}^{s}-\dfrac{B_{66}\cos\varphi_i}{R_{0i}}B_{i1}^{s}\\
\qquad=A_{66}\sum_{m=1}^{M}\varsigma_{Mm}^{s(1)}U_{im}^{x}+A_{66}\sum_{k=1}^{N}\varsigma_{ik}^{x(1)}U_{kM}^{s}-\dfrac{A_{66}\cos\varphi_i}{R_{0i}}U_{iM}^{s}\\
\qquad\quad+B_{66}\sum_{m=1}^{M}\varsigma_{Mm}^{s(1)}B_{im}^{x}+B_{66}\sum_{k=1}^{N}\varsigma_{ik}^{x(1)}B_{kM}^{s}-\dfrac{B_{66}\cos\varphi_i}{R_{0i}}B_{iM}^{s}\\
A_{12}\sum_{k=1}^{N}\varsigma_{ik}^{x(1)}U_{k1}^{x}+\dfrac{A_{22}\cos\varphi_i}{R_{0i}}U_{i1}^{x}+A_{11}\sum_{m=1}^{M}\varsigma_{1m}^{s(1)}U_{im}^{s}+\dfrac{A_{11}\sin\varphi_i}{R_{0i}}W_{i1}\\
\quad+B_{12}\sum_{k=1}^{N}\varsigma_{ik}^{x(1)}B_{k1}^{x}+\dfrac{B_{11}\cos\varphi_i}{R_{0i}}B_{i1}^{x}+B_{11}\sum_{m=1}^{M}\varsigma_{1m}^{s(1)}B_{im}^{s}\\
\qquad=A_{12}\sum_{k=1}^{N}\varsigma_{ik}^{x(1)}U_{kM}^{x}+\dfrac{A_{11}\cos\varphi_i}{R_{0i}}U_{iM}^{x}+A_{11}\sum_{m=1}^{M}\varsigma_{Mm}^{s(1)}U_{im}^{s}+\dfrac{A_{11}\sin\varphi_i}{R_{0i}}W_{iM}\\
\qquad\quad+B_{12}\sum_{k=1}^{N}\varsigma_{ik}^{x(1)}B_{kM}^{x}+\dfrac{B_{11}\cos\varphi_i}{R_{0i}}B_{iM}^{x}+B_{11}\sum_{m=1}^{M}\varsigma_{Mm}^{s(1)}B_{im}^{s}\\
\quad\kappa A_{66}\sum_{k=1}^{N}\varsigma_{ik}^{x(1)}W_{k1}+\kappa A_{66}B_{i1}^{x}+\kappa A_{66}B_{i1}^{s}\\
=\kappa A_{66}\sum_{k=1}^{N}\varsigma_{ik}^{x(1)}W_{kM}+\kappa A_{66}B_{iM}^{x}+\kappa A_{66}B_{iM}^{s}\\
B_{66}\sum_{m=1}^{M}\varsigma_{1m}^{s(1)}U_{im}^{\varphi}+B_{66}\sum_{k=1}^{N}\varsigma_{ik}^{x(1)}U_{k1}^{s}-\dfrac{B_{66}\cos\varphi_i}{R_{0i}}U_{i1}^{s}\\
\quad+D_{66}\sum_{m=1}^{M}\varsigma_{1m}^{s(1)}B_{im}^{x}+D_{66}\sum_{k=1}^{N}\varsigma_{ik}^{x(1)}B_{k1}^{s}-\dfrac{D_{66}\cos\varphi_i}{R_{0i}}B_{i1}^{s}\\
\qquad=B_{66}\sum_{m=1}^{M}\varsigma_{Mm}^{s(1)}U_{im}^{x}+B_{66}\sum_{k=1}^{N}\varsigma_{ik}^{x(1)}U_{kM}^{s}-\dfrac{B_{66}\cos\varphi_i}{R_{0i}}U_{iM}^{s}\\
\qquad\quad+D_{66}\sum_{m=1}^{M}\varsigma_{Mm}^{s(1)}B_{im}^{x}+D_{66}\sum_{k=1}^{N}\varsigma_{ik}^{x(1)}B_{kM}^{s}-\dfrac{D_{66}\cos\varphi_i}{R_{0i}}B_{iM}^{s}\\
B_{12}\sum_{k=1}^{N}\varsigma_{ik}^{x(1)}U_{k1}^{x}+\dfrac{B_{11}\cos\varphi_i}{R_{0i}}U_{i1}^{x}+B_{11}\sum_{m=1}^{M}\varsigma_{1m}^{s(1)}U_{im}^{s}+\dfrac{B_{11}\sin\varphi_i}{R_{0i}}W_{i1}\\
\quad+D_{12}\sum_{k=1}^{N}\varsigma_{ik}^{x(1)}B_{k1}^{x}+\dfrac{D_{11}\cos\varphi_i}{R_{0i}}B_{i1}^{x}+D_{11}\sum_{m=1}^{M}\varsigma_{1m}^{s(1)}B_{im}^{s}\\
\qquad=B_{12}\sum_{k=1}^{N}\varsigma_{ik}^{x(1)}U_{kM}^{x}+\dfrac{B_{11}\cos\varphi_i}{R_{0i}}U_{iM}^{x}+B_{11}\sum_{m=1}^{M}\varsigma_{Mm}^{s(1)}U_{im}^{s}+\dfrac{B_{11}\sin\varphi_i}{R_{0i}}W_{iM}\\
\qquad\quad+D_{12}\sum_{k=1}^{N}\varsigma_{ik}^{x(1)}B_{kM}^{x}+\dfrac{D_{11}\cos\varphi_i}{R_{0i}}B_{iM}^{x}+D_{11}\sum_{m=1}^{M}\varsigma_{Mm}^{s(1)}B_{im}^{s}\qquad\text{for } i=2,\ldots,N-1
\end{cases}
\tag{69}
$$

4.3. Solution procedure

Applying the GDQ procedure enables one to write the equations of motion in discrete form, transforming any space derivative into a weighted sum of node values of dependent variables. Thus, the whole system of differential equations has

Table 1
Physical parameters used in the analysis of free vibrations of the homogeneous isotropic structures ($p=\infty$).

Physical parameter	Value
Density of mass $\rho=\rho_M$	7800 kg/m^3
Young's modulus $E=E_M$	2.1×10^{11} Pa
Poisson coefficient $v=v_M$	0.3

Table 2
The first 10 frequencies for the conical panel C–F–F–F.

Frequencies (Hz)	GDQ method	Abaqus	Ansys	Nastran	Straus	Pro/Mechanica
f_1	76.80	77.06	77.12	77.23	76.99	77.06
f_2	106.53	106.84	107.15	106.92	106.89	106.82
f_3	152.17	152.54	152.63	152.82	152.14	152.54
f_4	187.12	187.94	188.31	188.57	187.64	187.92
f_5	248.57	249.37	250.60	250.21	249.39	249.30
f_6	262.12	261.46	262.79	262.36	261.40	261.45
f_7	308.50	308.37	308.97	309.19	307.24	308.34
f_8	345.90	346.86	348.48	348.68	346.45	346.86
f_9	380.15	379.80	382.67	381.47	380.08	379.99
f_{10}	400.73	401.52	404.08	403.66	401.78	401.50

Table 3
The first 10 frequencies for the cylindrical panel C–F–F–F.

Frequencies (Hz)	GDQ method	Abaqus	Ansys	Nastran	Straus	Pro/Mechanica
f_1	58.32	58.91	58.84	59.01	58.97	58.92
f_2	90.62	91.82	91.94	91.84	91.77	91.79
f_3	146.35	144.59	145.21	144.99	145.08	144.59
f_4	230.72	232.46	233.09	233.32	232.34	232.46
f_5	263.63	266.07	267.33	267.19	266.62	266.07
f_6	278.56	278.88	278.98	278.78	278.47	278.69
f_7	339.43	338.80	342.11	340.93	341.58	338.81
f_8	430.81	427.44	429.12	428.59	427.02	427.25
f_9	489.26	488.07	493.18	491.86	491.01	488.22
f_{10}	511.30	512.94	517.49	517.13	514.68	513.06

Table 4
The first 10 frequencies for the annular panel C–F–F–F.

Frequencies (Hz)	GDQ method	Abaqus	Ansys	Nastran	Straus	Pro/Mechanica
f_1	60.36	60.37	60.44	60.42	60.40	60.42
f_2	131.86	131.82	132.12	132.22	132.01	132.07
f_3	241.48	241.51	242.79	242.64	242.29	241.75
f_4	278.48	278.50	280.06	279.76	279.36	278.75
f_5	363.05	363.07	365.49	365.56	364.81	363.60
f_6	410.96	410.89	414.08	413.56	412.09	411.89
f_7	544.02	544.04	549.38	548.91	547.93	544.62
f_8	597.35	597.44	603.81	602.43	599.55	599.12
f_9	681.37	681.43	689.79	688.57	686.32	682.03
f_{10}	754.15	754.21	763.97	763.10	760.43	755.49

Table 5
The first 10 frequencies for the conical dome C–F.

Frequencies (Hz)	GDQ method	Abaqus	Ansys	Nastran	Straus	Pro/Mechanica
f_1	200.69	200.52	200.59	200.74	200.29	200.47
f_2	200.69	200.52	200.59	200.74	200.29	200.47
f_3	221.65	221.28	221.82	221.52	221.26	221.32
f_4	221.65	221.28	221.82	221.52	221.26	221.34
f_5	274.77	275.35	275.35	274.55	274.71	274.96
f_6	274.77	275.35	275.35	274.55	274.71	275.07
f_7	308.30	308.38	308.26	308.24	308.05	308.22
f_8	308.30	308.38	308.26	308.24	308.05	308.22
f_9	341.16	340.08	340.53	340.49	339.52	340.04
f_{10}	341.16	340.08	340.53	340.49	339.52	340.05

Table 6
The first 10 frequencies for the cylinder C–F.

Frequencies (Hz)	GDQ method	Abaqus	Ansys	Nastran	Straus	Pro/Mechanica
f_1	146.17	144.82	145.02	144.96	144.88	144.81
f_2	146.17	144.82	145.02	144.96	144.88	144.81
f_3	210.32	208.81	209.58	209.45	209.52	208.82
f_4	210.32	208.81	209.58	209.45	209.52	208.83
f_5	242.55	242.61	242.69	242.43	242.53	242.42
f_6	242.55	242.61	242.69	242.43	242.53	242.42
f_7	366.58	365.52	367.97	367.57	367.72	365.58
f_8	366.58	365.52	367.97	367.57	367.72	365.60
f_9	401.91	403.17	402.74	402.42	402.78	402.45
f_{10}	412.36	408.28	411.12	409.57	410.08	408.25

Table 7
The first 10 frequencies for the annular plate C–F.

Frequencies (Hz)	GDQ method	Abaqus	Ansys	Nastran	Straus	Pro/Mechanica
f_1	67.03	67.03	67.09	67.07	67.07	67.02
f_2	121.86	121.86	122.02	122.08	122.01	121.99
f_3	121.86	121.86	122.02	122.08	122.01	121.99
f_4	203.17	203.17	203.71	203.63	203.70	203.18
f_5	203.17	203.17	203.71	203.63	203.70	203.18
f_6	283.85	283.85	285.44	285.22	285.19	283.85
f_7	302.85	302.85	304.12	303.81	304.09	302.91
f_8	302.85	302.85	304.12	303.81	304.09	302.91
f_9	340.65	340.65	342.59	342.54	342.33	341.12
f_{10}	340.65	340.65	342.59	342.54	342.33	341.12

Table 8
The first 10 frequencies for conical shells characterized by different boundary conditions.

Frequencies (Hz)	Conical panel			Conical dome		
	C–F–C–F	F–S–F–S	S–S–F–F	C–C	S–S	C–S
f_1	122.73	74.28	90.92	227.59	208.69	225.59
f_2	135.28	125.33	170.04	227.59	208.69	225.59
f_3	241.48	224.79	232.33	239.71	222.70	234.82
f_4	256.59	258.79	272.43	239.71	222.70	234.82
f_5	287.24	288.70	312.85	275.27	250.33	275.11
f_6	293.42	327.04	324.61	275.27	250.33	275.11
f_7	381.19	360.93	374.71	333.69	318.11	331.96
f_8	421.65	388.22	411.13	333.69	318.11	331.96
f_9	463.67	444.46	454.88	350.59	318.66	350.58
f_{10}	494.98	480.42	488.36	350.59	318.66	350.58

Table 9
The first 10 frequencies for cylindrical shells characterized by different boundary conditions.

Frequencies (Hz)	Cylindrical panel			Cylinder		
	C–F–C–F	F–S–F–S	S–S–F–F	C–C	S–S	C–S
f_1	204.87	168.18	76.18	360.36	331.15	344.78
f_2	222.97	364.40	188.14	360.36	331.15	344.78
f_3	383.58	407.33	232.26	375.86	348.46	361.52
f_4	441.11	421.67	285.37	375.86	348.46	361.52
f_5	467.98	634.29	428.84	463.29	440.86	451.18
f_6	474.78	651.69	467.63	463.29	440.86	451.18
f_7	715.01	717.89	537.52	523.55	508.07	515.53
f_8	719.14	781.15	573.73	523.55	508.07	515.53
f_9	725.44	792.79	673.55	646.56	596.25	628.74
f_{10}	736.76	806.95	731.76	646.56	596.25	628.74

Table 10
The first 10 frequencies for annular plates characterized by different boundary conditions.

Frequencies (Hz)	Annular panel			Annular plate		
	C–F–C–F	F–S–F–S	S–S–F–F	C–C	S–S	C–S
f_1	235.47	13.52	57.68	238.05	115.42	182.68
f_2	249.30	76.326	150.27	246.01	129.88	196.69
f_3	307.53	159.11	233.13	246.01	129.88	196.69
f_4	424.25	167.87	288.57	275.54	175.58	242.03
f_5	592.67	287.65	401.53	275.54	175.58	242.03
f_6	628.39	315.23	456.92	335.89	250.65	319.28
f_7	648.64	399.78	588.04	335.89	250.65	319.28
f_8	729.72	434.01	619.55	427.31	347.67	421.25
f_9	795.34	505.97	650.91	427.31	347.67	421.25
f_{10}	876.77	604.97	763.19	542.01	432.75	540.29

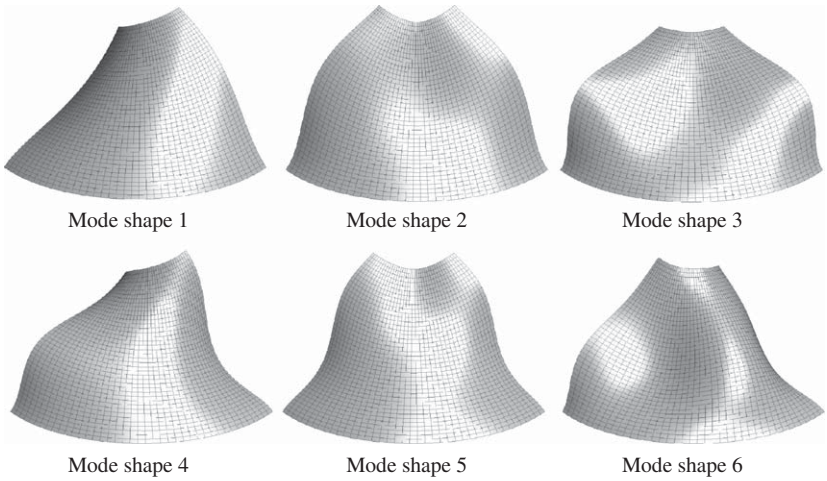

Fig. 5. Mode shapes for the conical panel C–F–F–F.

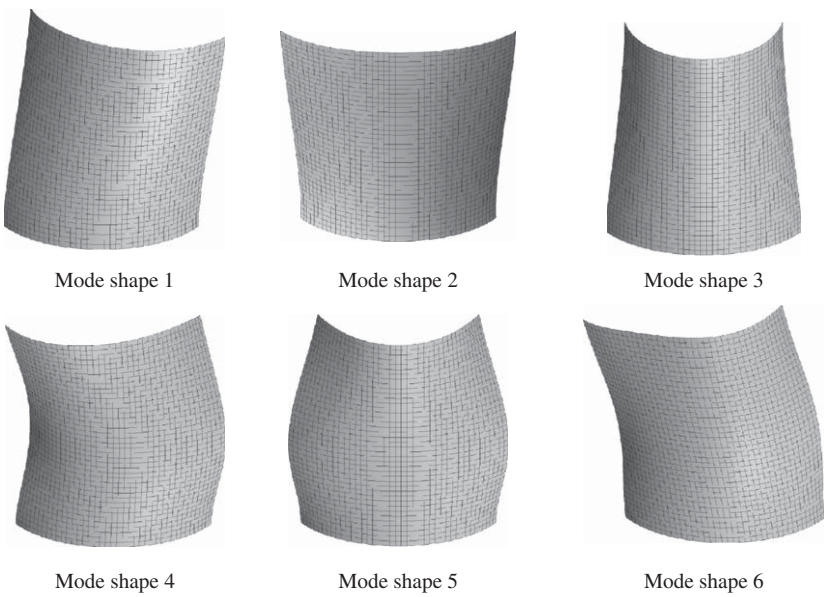

Fig. 6. Mode shapes for the cylindrical panel C–F–F–F.

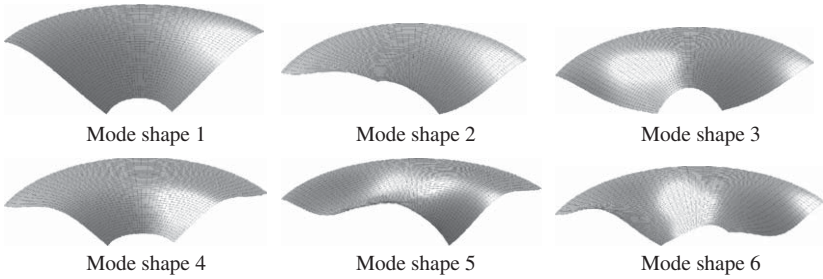

Fig. 7. Mode shapes for the annular panel C–F–F–F.

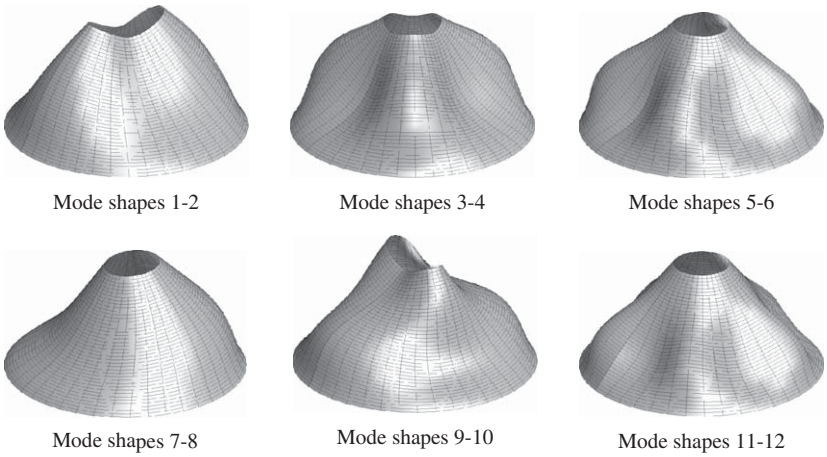

Fig. 8. Mode shapes for the conical dome C–F.

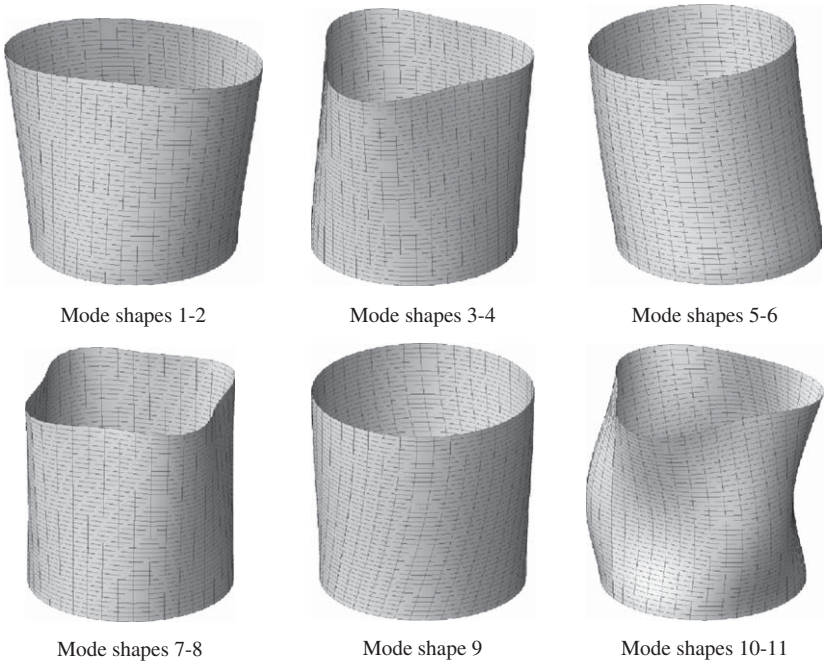

Fig. 9. Mode shapes for the cylinder C–F.

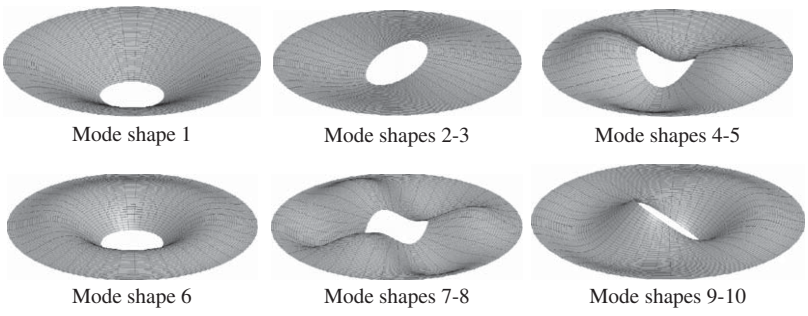

Fig. 10. Mode shapes for the annular plate C–F.

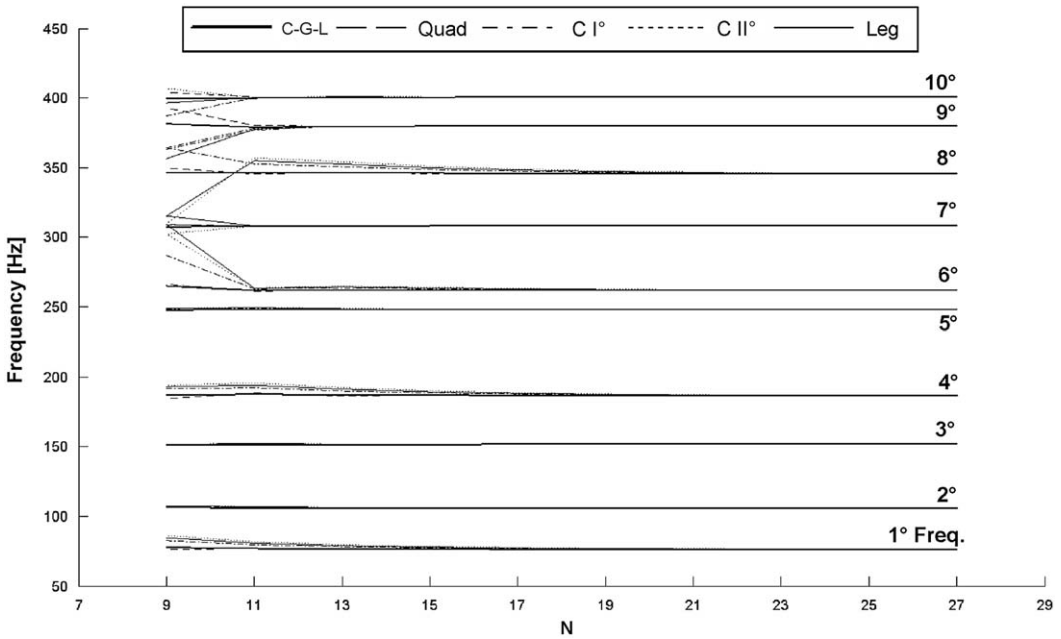

Fig. 11. Convergence and stability characteristics of the first 10 frequencies for the conical panel C–F–F–F using different typical grid distributions.

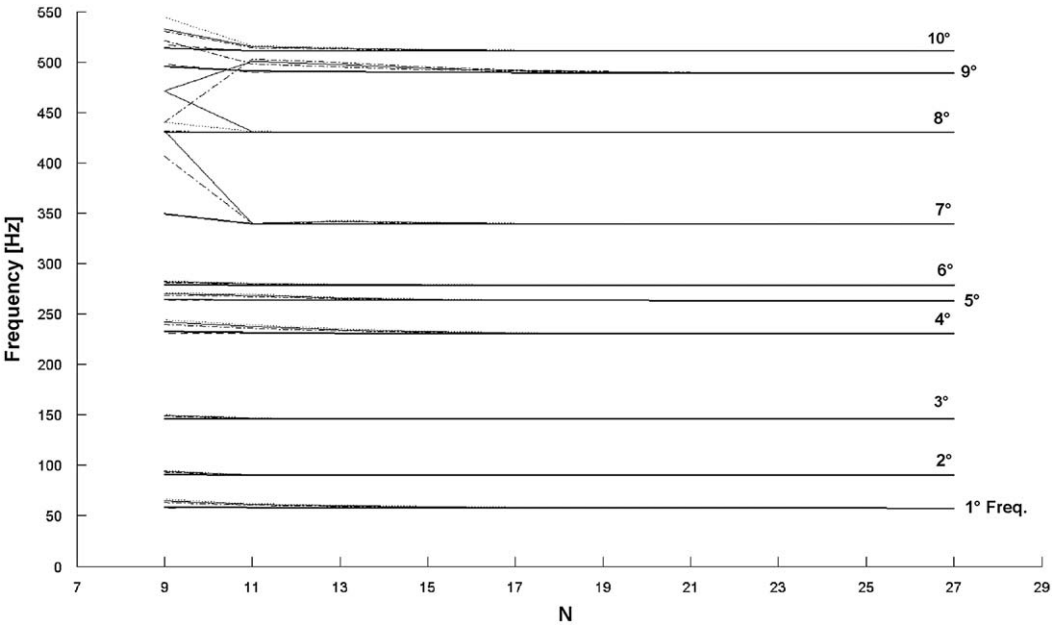

Fig. 12. Convergence and stability characteristics of the first 10 frequencies for the cylindrical panel C–F–F–F using different typical grid distributions.

been discretized and the global assembling leads to the following set of linear algebraic equations:

$$\left[\begin{array}{c|c} \mathbf{K}_{bb} & \mathbf{K}_{bd} \\ \hline \mathbf{K}_{db} & \mathbf{K}_{dd} \end{array}\right]\left[\begin{array}{c} \boldsymbol{\delta}_b \\ \hline \boldsymbol{\delta}_d \end{array}\right] = \omega^2 \left[\begin{array}{c|c} \mathbf{0} & \mathbf{0} \\ \hline \mathbf{0} & \mathbf{M}_{dd} \end{array}\right]\left[\begin{array}{c} \boldsymbol{\delta}_b \\ \hline \boldsymbol{\delta}_d \end{array}\right] \tag{70}$$

In the above matrices and vectors, the partitioning is set forth by subscripts *b* and *d*, referring to the system degrees of freedom and standing for *boundary* and *domain*, respectively. In this sense, the *b*-equations represent the discrete boundary and compatibility conditions, which are valid only for the points lying on constrained edges of the shell; while

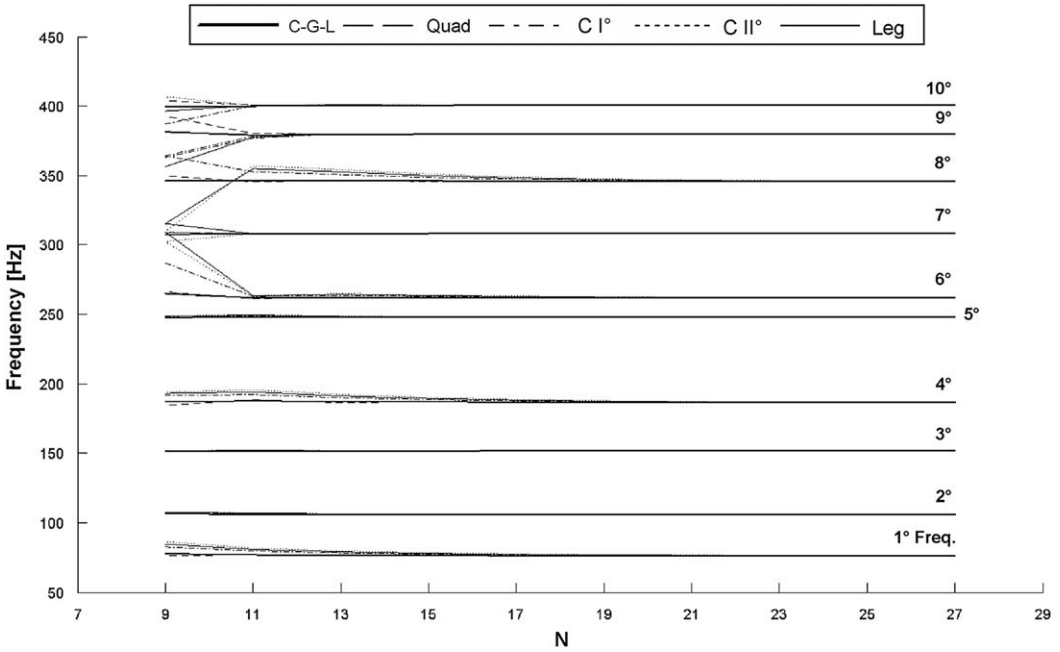

Fig. 13. Convergence and stability characteristics of the first 10 frequencies for the annular panel C–F–F–F using different typical grid distributions.

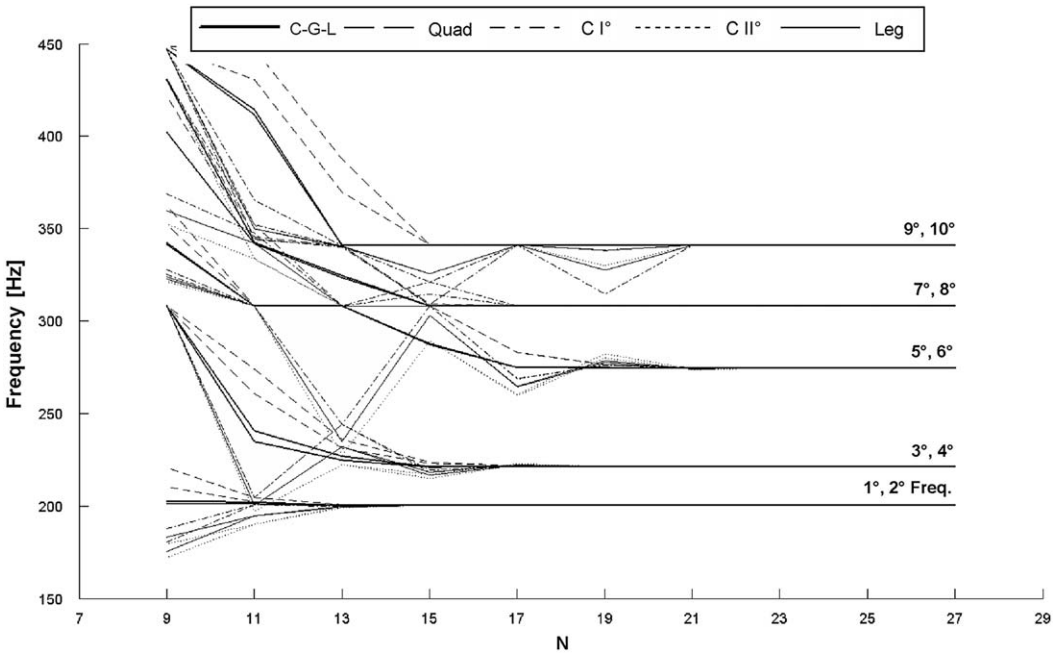

Fig. 14. Convergence and stability characteristics of the first 10 frequencies for the conical dome C–F using different typical grid distributions.

the *d*-equations are the equilibrium equations, assigned on interior nodes. In order to make the computation more efficient, kinematic condensation of non-domain degrees of freedom is performed

$$(\mathbf{K}_{dd} - \mathbf{K}_{db}(\mathbf{K}_{bb})^{-1}\mathbf{K}_{bd})\boldsymbol{\delta}_d = \omega^2 \mathbf{M}_{dd}\boldsymbol{\delta}_d \tag{71}$$

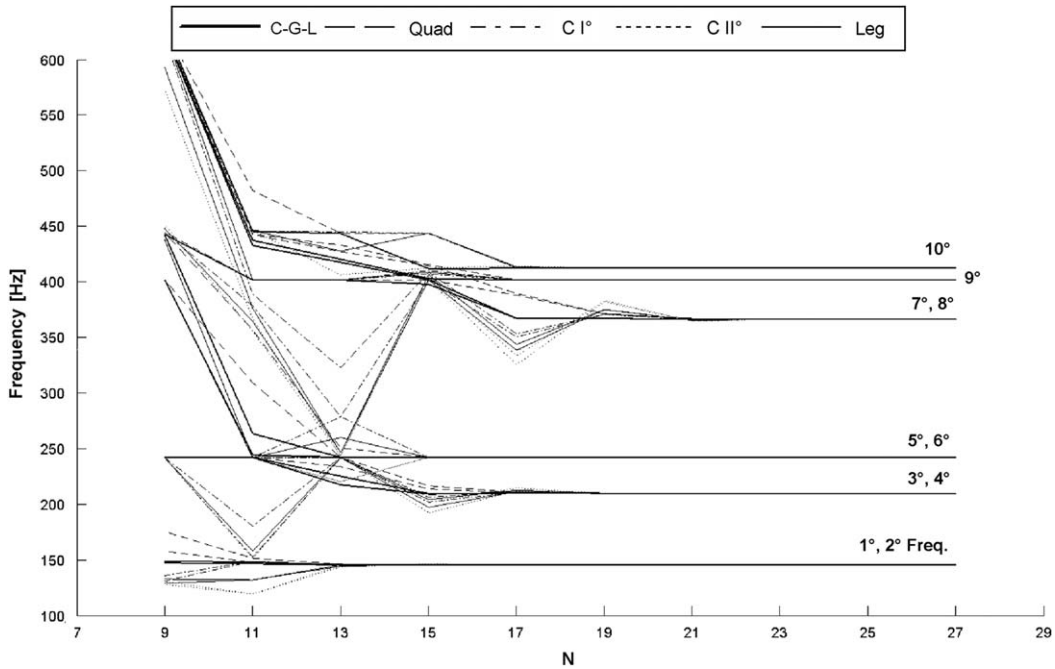

Fig. 15. Convergence and stability characteristics of the first 10 frequencies for the cylinder C–F using different typical grid distributions.

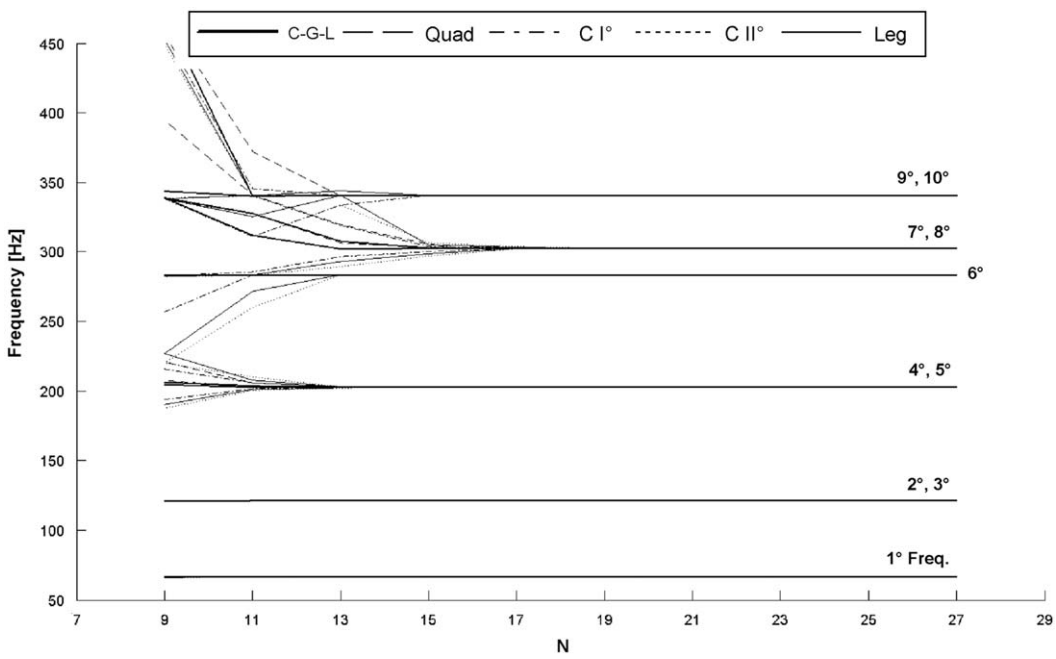

Fig. 16. Convergence and stability characteristics of the first 10 frequencies for the annular plate C–F using different typical grid distributions.

The natural frequencies of the structure considered can be determined by solving the standard eigenvalue problem (71). In particular, the solution procedure by means of GDQ technique has been implemented in a MATLAB code. Finally, the results in terms of frequencies are obtained using the *eigs* function of MATLAB program.

It is worth noting that, with the present approach, differing from the finite element method, no integration occurs prior to the global assembly of the linear system, and this results in a further computational cost saving in favor of the differential quadrature technique.

Table 11
The first 10 frequencies for the FGM_1 functionally graded conical panel C–F–F–F varying the power-law exponent p.

Material properties: $E_C = 168\,\text{GPa}$, $\nu_C = 0.3$, $\rho_C = 5700\,\text{kg/m}^3$, $E_M = 70\,\text{GPa}$, $\nu_M = 0.3$, $\rho_M = 2707\,\text{kg/m}^3$								
Frequencies (Hz)	$p=0$	$p=0.6$	$p=1$	$p=5$	$p=20$	$p=50$	$p=100$	$p=\infty$
f_1	80.36	78.18	77.81	78.96	77.75	76.55	75.97	75.27
f_2	111.46	109.02	108.45	108.27	106.66	105.56	105.04	104.39
f_3	159.21	154.95	154.18	156.11	153.83	151.52	150.43	149.13
f_4	195.79	189.60	188.71	193.10	190.29	186.97	185.35	183.39
f_5	260.08	253.29	252.08	254.47	250.65	247.27	245.63	243.61
f_6	274.26	265.15	263.94	271.26	267.32	262.30	259.86	256.89
f_7	322.79	314.65	313.01	315.45	310.93	306.68	304.69	302.34
f_8	361.92	350.18	348.48	356.75	351.74	345.63	342.64	338.99
f_9	397.75	383.33	381.61	394.62	388.98	381.16	377.29	372.56
f_{10}	419.29	407.61	405.64	408.06	402.09	399.22	396.29	392.73

Table 12
The first 10 frequencies for the FGM_1 functionally graded conical dome C–F varying the power-law exponent p.

Material properties: $E_C = 168\,\text{GPa}$, $\nu_C = 0.3$, $\rho_C = 5700\,\text{kg/m}^3$, $E_M = 70\,\text{GPa}$, $\nu_M = 0.3$, $\rho_M = 2707\,\text{kg/m}^3$								
Frequencies (Hz)	$p=0$	$p=0.6$	$p=1$	$p=5$	$p=20$	$p=50$	$p=100$	$p=\infty$
f_1	209.99	205.96	204.91	203.93	200.79	198.73	197.79	196.69
f_2	209.99	205.96	204.91	203.93	200.79	198.73	197.79	196.69
f_3	231.96	225.52	224.44	227.67	224.29	220.86	219.21	217.23
f_4	231.96	225.52	224.44	227.67	224.29	220.86	219.21	217.23
f_5	287.48	277.93	276.66	284.26	280.15	274.93	272.38	269.28
f_6	287.48	277.93	276.66	284.26	280.15	274.93	272.38	269.28
f_7	322.57	318.18	316.32	309.57	305.04	303.46	302.83	302.14
f_8	322.57	318.18	316.32	309.57	305.04	303.46	302.83	302.14
f_9	356.95	349.48	347.66	347.08	341.87	338.11	336.39	334.35
f_{10}	356.95	349.48	347.66	347.08	341.87	338.11	336.39	334.35

Table 13
The first 10 frequencies for the FGM_1 functionally graded cylindrical panel C–F–F–F varying the power-law exponent p.

Material properties: $E_C = 168\,\text{GPa}$, $\nu_C = 0.3$, $\rho_C = 5700\,\text{kg/m}^3$, $E_M = 70\,\text{GPa}$, $\nu_M = 0.3$, $\rho_M = 2707\,\text{kg/m}^3$								
Frequencies (Hz)	$p=0$	$p=0.6$	$p=1$	$p=5$	$p=20$	$p=50$	$p=100$	$p=\infty$
f_1	61.02	59.24	58.96	60.09	59.19	58.20	57.73	57.16
f_2	94.82	93.14	92.65	91.69	90.29	89.55	89.21	88.81
f_3	153.13	148.51	147.94	152.02	149.49	146.55	145.14	143.43
f_4	241.39	234.79	233.64	236.75	233.27	229.79	228.12	226.11
f_5	275.83	267.06	265.86	272.42	268.37	263.58	261.23	258.36
f_6	291.46	287.85	286.16	279.34	275.23	273.98	273.51	273.00
f_7	355.14	343.22	342.08	354.89	348.80	341.04	337.25	332.65
f_8	450.76	443.06	440.72	436.34	429.63	425.83	424.15	422.21
f_9	511.92	495.89	493.67	505.35	497.87	489.06	484.75	479.49
f_{10}	534.97	517.96	515.48	527.38	519.85	510.86	506.45	501.09

5. Applications and results

In the present paragraph, some results and considerations about the free vibration problem of conical, cylindrical shells and annular plates are presented. The analysis has been carried out by means of numerical procedures illustrated previously. The details regarding the geometry of the structures considered are indicated below:

- *Conical panel*: $R_i = 0.5\,\text{m}$, $h = 0.1\,\text{m}$, $L = 2\,\text{m}$, $\alpha = 40^\circ$, $\vartheta_0 = 120^\circ$ (Tables 2, 8 and 11);
- *Conical dome*: $R_i = 0.5\,\text{m}$, $h = 0.1\,\text{m}$, $L = 2\,\text{m}$, $\alpha = 40^\circ$, $\vartheta_0 = 120^\circ$ (Tables 5, 8 and 12);
- *Cylindrical panel*: $R_i = 1\,\text{m}$, $h = 0.1\,\text{m}$, $L = 2\,\text{m}$, $\alpha = 0^\circ$, $\vartheta_0 = 120^\circ$ (Tables 3, 9 and 13);
- *Cylinder*: $R_i = 1\,\text{m}$, $h = 0.1\,\text{m}$, $L = 2\,\text{m}$, $\alpha = 0^\circ$, $\vartheta_0 = 360^\circ$ (Tables 6, 9 and 14);

Table 14
The first 10 frequencies for the FGM_1 functionally graded cylinder C–F varying the power-law exponent p.

Material properties: $E_C = 168\,\text{GPa}$, $\nu_C = 0.3$, $\rho_C = 5700\,\text{kg/m}^3$, $E_M = 70\,\text{GPa}$, $\nu_M = 0.3$, $\rho_M = 2707\,\text{kg/m}^3$

Frequencies (Hz)	$p=0$	$p=0.6$	$p=1$	$p=5$	$p=20$	$p=50$	$p=100$	$p=\infty$
f_1	152.93	150.03	149.29	148.75	146.38	144.80	144.09	143.25
f_2	152.93	150.03	149.29	148.75	146.38	144.80	144.09	143.25
f_3	220.06	212.94	212.22	219.49	215.71	211.09	208.85	206.12
f_4	220.06	212.94	212.22	219.49	215.71	211.09	208.85	206.12
f_5	253.78	250.74	249.31	243.43	239.74	238.60	238.17	237.71
f_6	253.78	250.74	249.31	243.43	239.74	238.60	238.17	237.71
f_7	383.55	370.63	369.46	383.71	377.01	368.49	364.33	359.26
f_8	383.55	370.63	369.46	383.71	377.02	368.49	364.33	359.26
f_9	420.51	415.47	412.97	402.56	396.70	395.08	394.49	393.88
f_{10}	431.45	420.39	418.46	423.57	416.96	410.69	407.71	404.13

Table 15
The first 10 frequencies for the FGM_1 functionally graded annular panel C–F–F–F varying the power-law exponent p.

Material properties: $E_C = 168\,\text{GPa}$, $\nu_C = 0.3$, $\rho_C = 5700\,\text{kg/m}^3$, $E_M = 70\,\text{GPa}$, $\nu_M = 0.3$, $\rho_M = 2707\,\text{kg/m}^3$

Frequencies (Hz)	$p=0$	$p=0.6$	$p=1$	$p=5$	$p=20$	$p=50$	$p=100$	$p=\infty$
f_1	63.16	60.46	60.15	62.71	61.97	60.64	59.97	59.16
f_2	137.96	132.18	131.49	136.83	135.21	132.38	130.96	129.22
f_3	252.66	242.12	240.85	250.52	247.55	242.40	239.83	236.66
f_4	291.38	279.25	277.78	288.87	285.44	279.52	276.56	272.92
f_5	379.86	364.35	362.42	376.17	371.69	364.18	360.42	355.80
f_6	429.98	412.41	410.23	425.82	420.75	412.24	407.98	402.75
f_7	569.21	546.17	543.26	563.38	556.66	545.55	539.99	533.16
f_8	625.01	599.91	596.71	618.33	610.95	598.88	592.85	585.43
f_9	712.91	684.37	680.72	705.14	696.74	683.04	676.19	667.77
f_{10}	789.06	757.90	753.83	779.88	770.56	755.68	748.24	739.09

Table 16
The first 10 frequencies for the FGM_1 functionally graded annular plate C–F varying the power-law exponent p.

Material properties: $E_C = 168\,\text{GPa}$, $\nu_C = 0.3$, $\rho_C = 5700\,\text{kg/m}^3$, $E_M = 70\,\text{GPa}$, $\nu_M = 0.3$, $\rho_M = 2707\,\text{kg/m}^3$

Frequencies (Hz)	$p=0$	$p=0.6$	$p=1$	$p=5$	$p=20$	$p=50$	$p=100$	$p=\infty$
f_1	70.13	67.13	66.78	69.64	68.81	67.34	66.59	65.68
f_2	127.49	122.13	121.49	126.49	124.98	122.35	121.04	119.42
f_3	127.49	122.13	121.49	126.49	124.98	122.35	121.04	119.42
f_4	212.58	203.65	202.59	210.87	208.36	203.99	201.80	199.12
f_5	212.58	203.65	202.59	210.87	208.36	203.99	201.80	199.12
f_6	296.99	284.62	283.12	294.46	290.96	284.92	281.89	278.18
f_7	316.87	303.70	302.11	314.12	310.38	303.96	300.75	296.80
f_8	316.87	303.70	302.11	314.12	310.38	303.96	300.75	296.80
f_9	356.42	341.79	339.99	353.06	348.86	341.76	338.21	333.85
f_{10}	356.42	341.79	339.99	353.06	348.86	341.76	338.21	333.85

- *Annular panel*: $R_i = 0.5\,\text{m}$, $h = 0.1\,\text{m}$, $R_e - R_i = 1.5\,\text{m}$, $\alpha = 90^\circ$, $\vartheta_0 = 120^\circ$, where R_e is the external radius (Tables 4, 10 and 15);
- *Annular plate*: $R_i = 0.5\,\text{m}$, $h = 0.1\,\text{m}$, $R_e - R_i = 1.5\,\text{m}$, $\alpha = 90^\circ$, $\vartheta_0 = 360^\circ$, where R_e is the external radius (Tables 7, 10 and 16).

The geometrical boundary conditions for the shell panel are identified by the following convention. For example, the symbolism C–S–C–F indicates that the edges $x = x_0$, $s = s_0$, $x = 0$, $s = 0$ are clamped, simply supported, clamped and free, respectively. For the complete shell of revolution, for example, the symbolism C–F indicates that the edges $x = x_0$ and $x = 0$ are clamped and free, respectively. In this case, the missing boundary conditions are the kinematic and physical compatibility conditions that are applied at the same meridian for $s = 0$ and $s_0 = 2\pi R_0$.

5.1. Homogeneous isotropic materials: GDQ convergence and stability characteristics

By considering the relations (16), when the power-law exponent is set equal to zero ($p = 0$) or equal to infinity ($p = \infty$), the homogeneous isotropic material is obtained as a special case of functionally graded material. In fact, from Eqs. (16), (15)

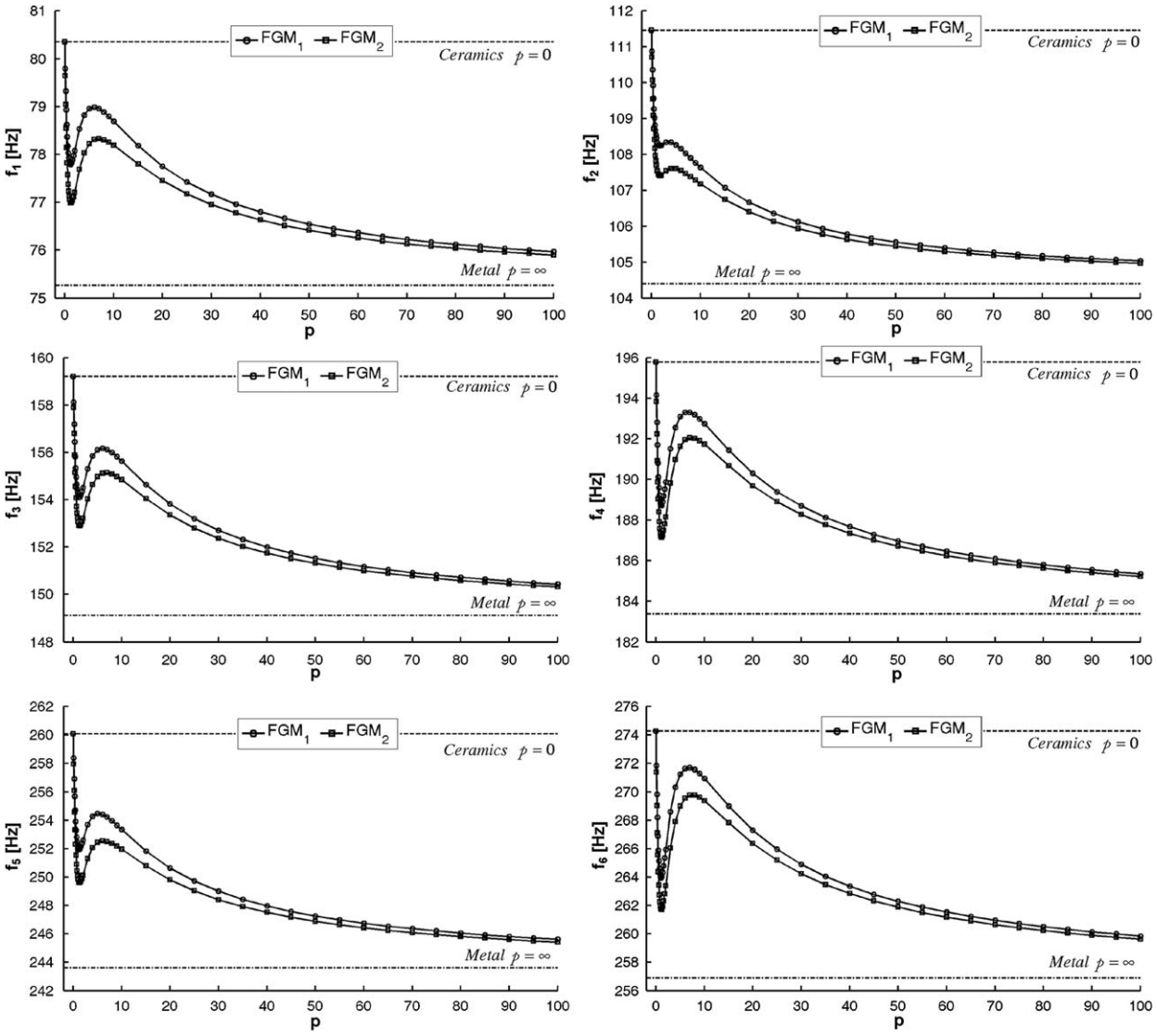

Fig. 17. Influence of the power-law exponent p and of the power-law distribution choice on the frequency characteristics of functionally graded conical panel C–F–F–F.

and (14) it is possible to obtain:

$$p = 0 \rightarrow V_C = 1, \quad V_M = 0 \rightarrow \rho(\zeta) = \rho_C, \quad E(\zeta) = E_C, \quad \nu(\zeta) = \nu_C$$

$$p = \infty \rightarrow V_C = 0, \quad V_M = 1 \rightarrow \rho(\zeta) = \rho_M, \quad E(\zeta) = E_M, \quad \nu(\zeta) = \nu_M \tag{72}$$

The mechanical characteristics for the homogeneous isotropic structures are listed in Table 1. In order to verify the accuracy of the numerical procedure, some comparisons have also been performed. The first 10 natural frequencies of conical, cylindrical shells and annular plates are reported in Tables 2–7. One of the aims of this paper is to compare results from the present analysis with those results obtained with finite element techniques and based on the same shell theory. In Tables 2–7, the results obtained by the GDQ method are compared with the FEM results obtained with commercial programs. For the GDQ results reported in Tables 2–7, we have considered the same C–G–L grid distribution with $N = 21$ and $M = 21$. For the commercial programs reported in Tables 2–7, we have used shell elements with eight nodes and well-converged and accurate results were obtained using 50×50 element meshes for the shell panels and 50×100 element meshes for the complete shells of revolution. It is noteworthy that the results from the present methodology are very close to those obtained by the commercial programs. As can be seen, the numerical results show an excellent agreement. Furthermore, it is significant that the computational effort in terms of time and number of grid points is smaller for the GDQ method results than for the finite element method. Some new results for the considered structures with different

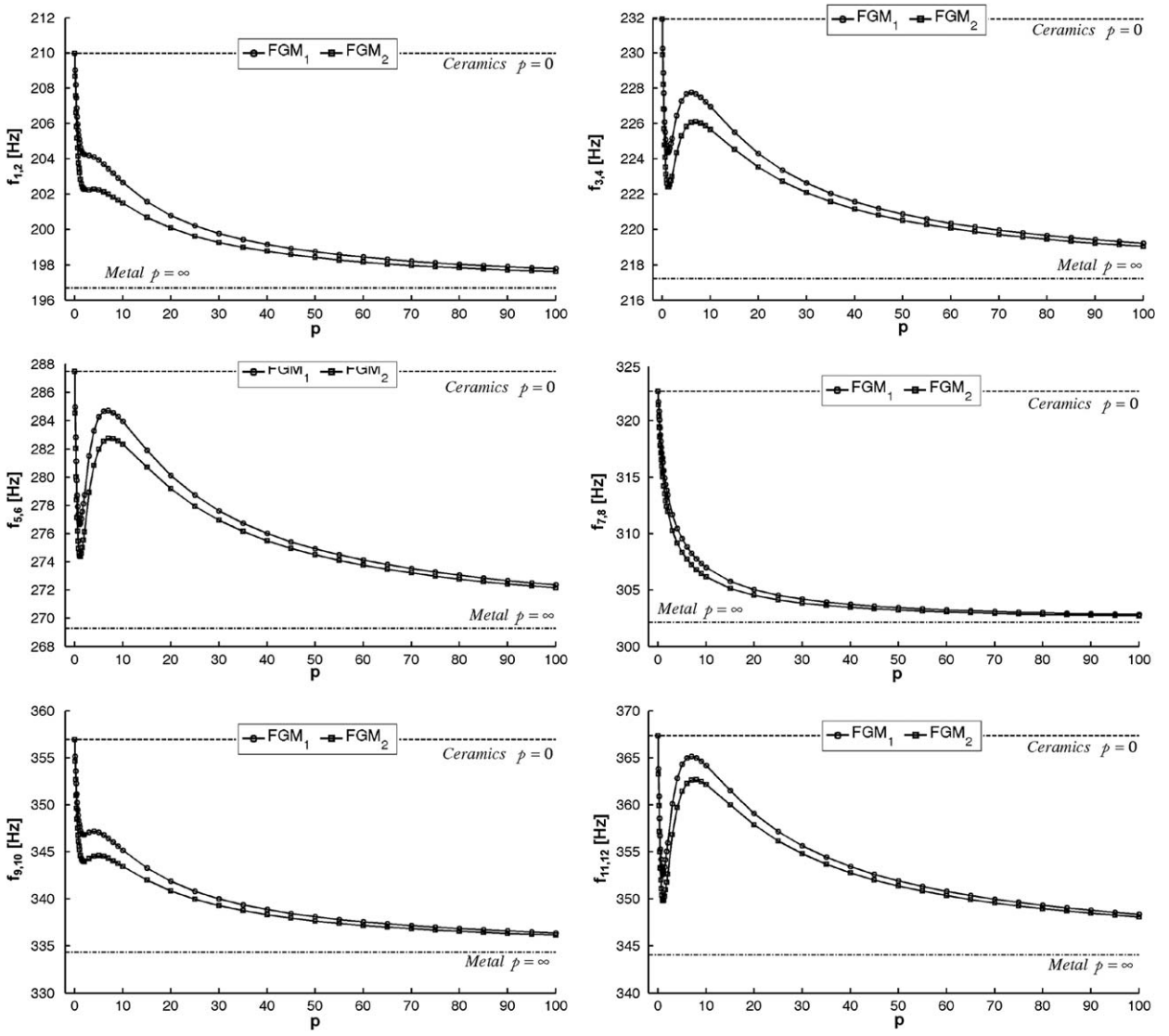

Fig. 18. Influence of the power-law exponent p and of the power-law distribution choice on the frequency characteristics of functionally graded conical dome C–F.

boundary conditions are exhibited in Tables 8–10. For these cases, we have also considered the same C–G–L grid distribution with $N = 21$ and $M = 21$. In Figs. 5–7, we have reported the first six mode shapes for the conical, cylindrical and annular panels characterized by C–F–F–F boundary conditions, while in Figs. 8–10 the mode shapes for the conical dome, cylinder and annular plate characterized by C–F boundary conditions are illustrated. In particular, for the conical dome, cylinder and annular plate, there are some symmetrical mode shapes due to the symmetry of the problem considered in 3D space. In these cases, we have summarized the symmetrical mode shapes only in one figure. The convergence and the stability of some natural frequencies for the structures under consideration with various grid distributions are shown in Figs. 11–16. Well convergent results for the frequencies can be obtained, if non-uniform grid point distributions are considered. In fact, the uniform grid distribution always presents less accurate results in comparison to non-uniform grids. It can be seen from the figures that the Chebyshev–Gauss–Lobatto (C–G–L) grid point distribution has the most rapid converging speed and provides more accurate solutions. Instead, the solutions obtained by using Chebyshev I° (C I°), Chebyshev II° (C II°), Legendre (Leg) and Quadratic (Quad) grid point distributions oscillate much more. It is shown that the solution accuracy of the non-uniform grid distributions stays steady with increasing $N = M$ and does not decrease due to the numerical instabilities even if $N = M$ becomes too large. For all the treated cases the non-uniform distributions are stable if the number of grid points increases. As shown in all the figures under consideration, to obtain accurate results for the higher frequencies the number of sampling points must not be large enough. Figs. 11–13 present the convergence characteristics of some frequencies for the conical, cylindrical and annular panels characterized by C–F–F–F boundary

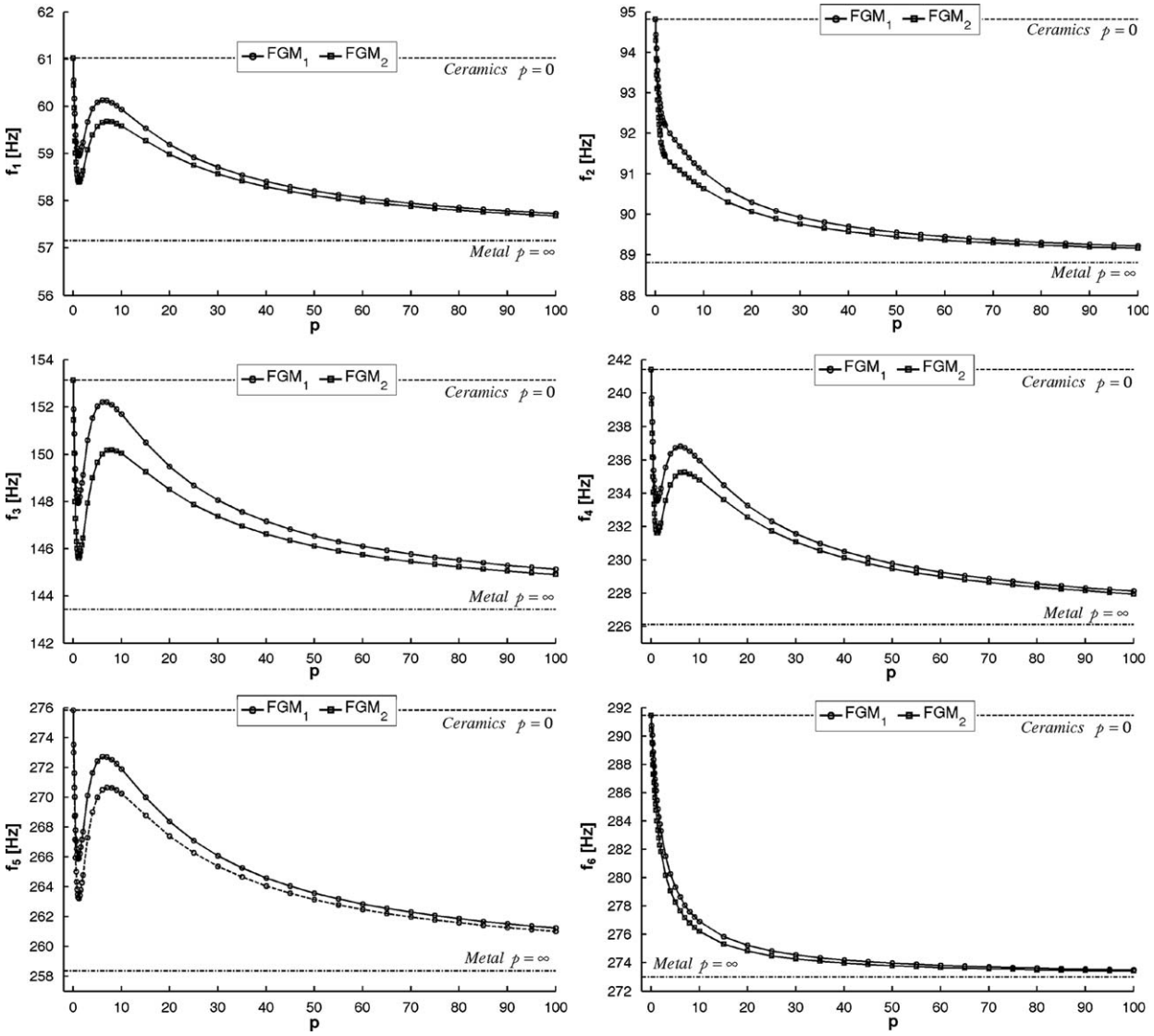

Fig. 19. Influence of the power-law exponent p and of the power-law distribution choice on the frequency characteristics of functionally graded cylindrical panel C–F–F–F.

conditions, while Figs. 14–16 show the convergence characteristics of some frequencies for the conical dome, cylinder and annular plate characterized by C–F boundary conditions. The boundary conditions influence the convergence and stability characteristics. In fact, it can be seen from these figures that the solutions for the conical, cylindrical and annular panels have the most rapid converging speed and provide more accurate results with a lower number of sampling points. Panel type structures yield very accurate results for the considered frequencies using the C–G–L grid distribution with $N = M = 17$. Instead, the worked solutions for the conical dome, cylinder and annular plate oscillate much more and require a larger number of sampling points. In these cases, compatibility conditions are introduced and must be implemented to solve the complete shell of revolution problem. To obtain accurate results for the higher frequencies, it is necessary to use a C–G–L grid distribution with $N = M = 21$ sampling points. In fact, these frequencies show the slower convergence rate. It is worth noting that, using all the non-uniform grid distributions, the methodology presents good stability and converging characteristics. Furthermore, the accuracy depends on the number of sampling points used.

5.2. Functionally graded materials

In the present paragraph, some results and considerations about the free vibration problem of FGM shells are presented. Regarding the functionally graded materials, their two constituents are taken to be zirconia (ceramic) and aluminum (metal), as can be seen from the mechanical characteristics listed in Tables 11–16. The details regarding the geometry of the

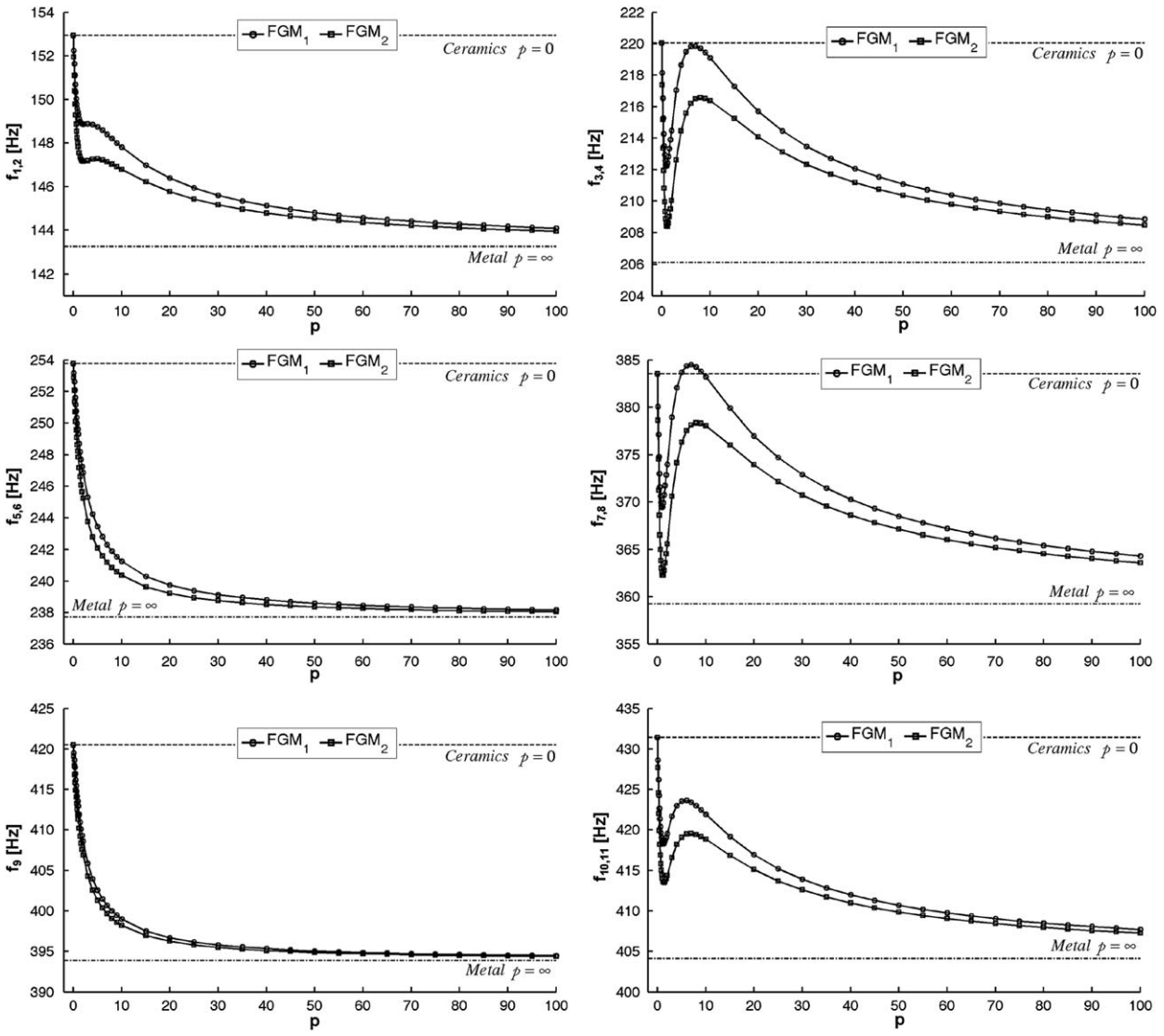

Fig. 20. Influence of the power-law exponent p and of the power-law distribution choice on the frequency characteristics of functionally graded cylinder C–F.

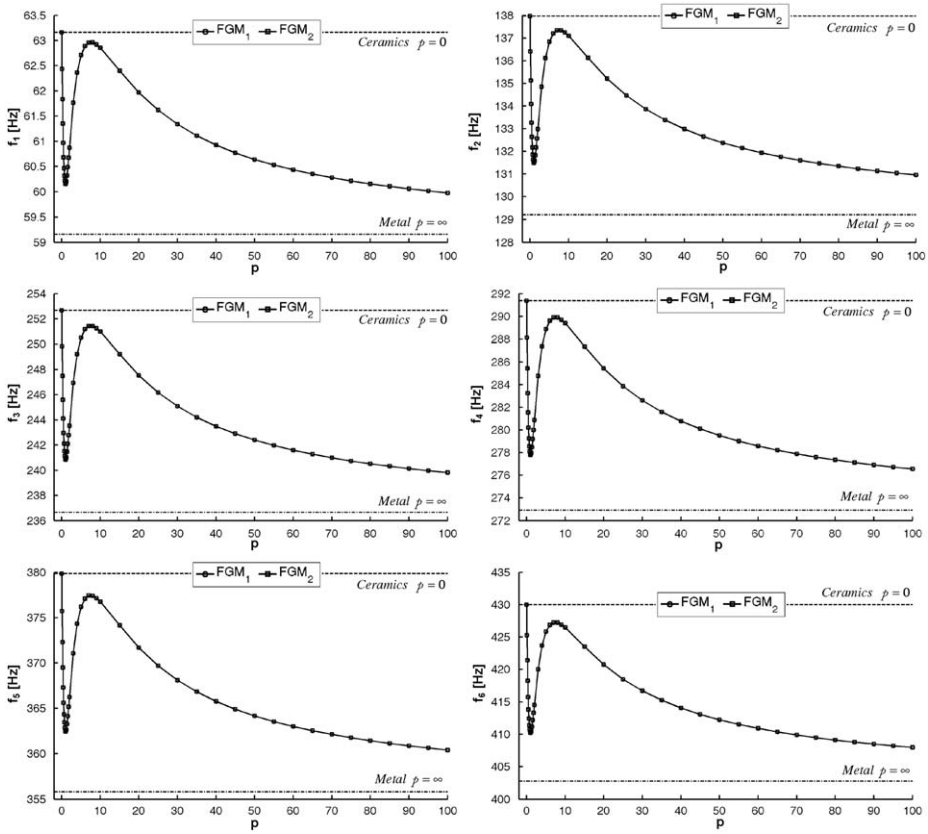

Fig. 21. Influence of the power-law exponent p and of the power-law distribution choice on the frequency characteristics of functionally graded annular panel C–F–F–F.

structures are presented previously. For the GDQ results, we have considered the Chebyshev–Gauss–Lobatto (C–G–L) grid distribution with $N = M = 31$. Tables 11–16 illustrate the results obtained using various values of the power-law exponent p (i.e. $p = 0$ ceramic rich and $p = \infty$ metallic rich) for the FGM_1 power-law distribution. These tables show how by varying the power-law index p of the volume fraction V_C it is possible to modify natural frequencies of FGM shells. The influence of the index p on the vibration frequencies is shown in Figs. 17–22. As can be seen from the figures, natural frequencies of FGM shell panels present an intermediate value between the natural frequencies of the limit cases of homogeneous shell panels of zirconia ($p = 0$) and of aluminum ($p = \infty$), as expected. It is interesting to note that the frequencies attain a minimum value for a shell made only of metal, due to the fact that aluminum has a much smaller Young's modulus that zirconia. In particular, it can be noted that the most of frequencies exhibits a fast descending behavior from the ceramic limit case ($p = 0$) varying the power-law index from $p = 0$ to 1, while for values of p greater than unity frequencies increase until a maximum value. After this maximum, frequencies slowly decrease by increasing the power-law exponent p and tend to the metallic limit case ($p = \infty$). This is expected because the more p increases the more the ceramic content is low and the FGM shell approaches the case of the fully metallic shell. The behavior described above is not present in all the frequencies and depends on the type of vibration mode. It is worth noting that in Figs. 18–20 some frequencies do not present the characteristic knee described above, but decrease gradually from the ceramic limit case ($p = 0$) to the metallic limit case ($p = \infty$) by increasing the power-law exponent p. In particular, the types of vibration mode that present this monotone gradually decrease of frequency are torsional and bending mode shapes, while the circumferential and radial mode shapes are characterized by a knee, as can be seen by comparing the mode shapes in Figs. 5–10 with Figs. 17–22. For examples, the frequencies f_7, f_8 of the conical dome of Fig. 18 and f_5, f_6 of the cylinder of Fig. 20 correspond to bending mode shapes as can be observed from Figs. 8 and 9, respectively, while the frequency f_9 of the cylinder of Fig. 20 correspond to a torsional mode shape as can be inferred from Fig. 9.

Furthermore, Figs. 17–22 also show the effect of the power-law distribution choice on the frequency parameters. As can be seen, the FGM_1 power-law frequency curves are always over the FGM_2 power-law frequency curves for any value of p. Moreover, the distance between these two curves increases with increasing the shell thickness because of the curvature of the shell. In fact, for curved shells it is important from dynamic vibration point of view to know if the top surface of the shell ($\zeta = h/2$) is ceramic or metallic rich and if the bottom surface ($\zeta = -h/2$) is metallic or ceramic rich.

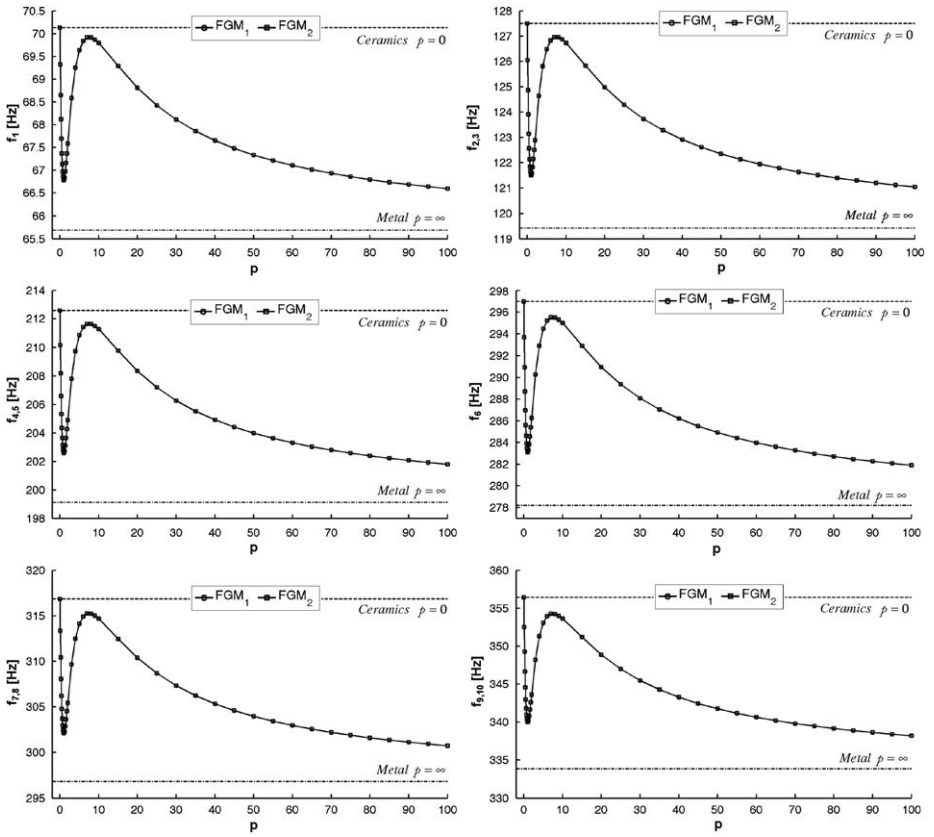

Fig. 22. Influence of the power-law exponent p and of the power-law distribution choice on the frequency characteristics of functionally graded annular plate C–F.

6. Conclusions

The generalized differential quadrature method has been used to study the free vibration analysis of functionally graded conical, cylindrical shells and annular plates. The adopted shell theory is the first-order shear deformation theory. Complete revolution shells are obtained as special cases of shell panels by satisfying the kinematic and physical compatibility.

In this study, ceramic–metallic graded shells of revolution with two different power-law variations of the volume fraction of the constituents in the thickness direction have been considered. The numerical results have shown the influence of the power-law exponent and of the power-law distribution choice on the free vibrations of functionally graded shells considered. For shells with zero curvature such as annular panels and plates, it has been shown that the power-law distribution choice on the free vibrations does not produce any effect from the dynamic vibration point of view. On the contrary, for curved shells such as cylindrical and conical panels and shells, it has been observed that the influence of the distribution choice is marked and can be considered from the structural design point of view. In general, it can be concluded that the frequency vibration of functionally graded shells depends on the type of vibration mode, thickness, power-law distribution, power-law exponent and curvature of the structure.

For the isotropic and homogeneous special case, numerical solutions has been compared with the ones obtained using commercial programs such as Abaqus, Ansys, Nastran, Straus, Pro/Mechanica. The comparisons conducted with FEM codes confirm how GDQ simple numerical method provides accurate and computationally low cost results for all the structures considered. Detailed convergence and comparison studies conducted have demonstrated the accuracy and stability of the proposed methodology.

Acknowledgments

This research was supported by the Italian Ministry for University and Scientific, Technological Research MIUR (40% and 60%). The research topic is one of the subjects of the Centre of Study and Research for the Identification of Materials and Structures (CIMEST)-"M. Capurso" of the University of Bologna (Italy).

References

[1] J.L. Sanders, An improved first approximation theory of thin shells, NASA TR-R24, Washington, DC, 1959.
[2] W. Flügge, *Stresses in Shells*, Springer, New York, 1960.
[3] V.V. Novozhilov, *Thin Shell Theory*, P. Noordhoff, Groningen, 1964.
[4] V.Z. Vlasov, General theory of shells and its application in engineering, NASA TTF-99, Washington, DC, 1964.
[5] H. Kraus, *Thin Elastic Shells*, Wiley, New York, 1967.
[6] A.W. Leissa, Vibration of shells, NASA SP-288, Washington, DC, 1973.
[7] F.I. Niordson, *Shell Theory*, North-Holland, Amsterdam, 1985.
[8] C. Shu, An efficient approach for free vibration analysis of conical shells, *Int. J. Mech. Sci.* 38 (1996) 935–949.
[9] K.Y. Lam, L. Hua, Vibration analysis of a rotating truncated circular conical shell, *Int. J. Solids Struct.* 34 (1997) 2183–2197.
[10] L. Hua, K.Y. Lam, Frequency characteristics of a thin rotating cylindrical shell using the generalized differential quadrature method, *Int. J. Mech. Sci.* 40 (1998) 443–459.
[11] T.Y. Ng, H. Li, K.Y. Lam, C.T. Loy, Parametric instability of conical shells by the generalized differential quadrature method, *Int. J. Numer. Meth. Eng.* 44 (1999) 819–837.
[12] L. Hua, K.Y. Lam, The generalized quadrature method for frequency analysis of a rotating conical shell with initial pressure, *Int. J. Numer. Meth. Eng.* 48 (2000) 1703–1722.
[13] K.Y. Lam, L. Hua, Influence of initial pressure on frequency characteristics of a rotating truncated circular conical shell, *Int. J. Mech. Sci.* 42 (2000) 213–236.
[14] L. Hua, K.Y. Lam, Orthotropic influence on frequency characteristics of rotating composite laminated conical shell by the generalized differential quadrature method, *Int. J. Solids Struct.* 38 (2001) 3995–4015.
[15] K.Y. Lam, H. Li, T.Y. Ng, C.F. Chua, Generalized differential quadrature method for the free vibration of truncated conical panels, *J. Sound Vib.* 251 (2002) 329–348.
[16] P.L. Gould, *Finite Element Analysis of Shells of Revolution*, Pitman Publishing, Boston, 1984.
[17] P.L. Gould, *Analysis of Plates and Shells*, Prentice-Hall, New Jersey, 1999.
[18] J.N. Reddy, *Mechanics of Laminated Composites Plates and Shells*, CRC Press, New York, 2003.
[19] E. Reissner, The effect of transverse shear deformation on the bending of elastic plates, *J. Appl. Mech. ASME* 12 (1945) 66–77.
[20] C. Shu, Free vibration analysis of composite laminated conical shells by generalized differential quadrature, *J. Sound Vib.* 194 (1996) 587–604.
[21] C.P. Wu, C.Y. Lee, Differential quadrature solution for the free vibration analysis of laminated conical shells with variable stiffness, *Int. J. Mech. Sci.* 43 (2001) 1853–1869.
[22] E. Viola, E. Artioli, The G.D.Q. method for the harmonic dynamic analysis of rotational shell structural elements, *Struct. Eng. Mech.* 17 (2004) 789–817.
[23] E. Artioli, E. Viola, Static analysis of shear-deformable shells of revolution via G.D.Q. method, *Struct. Eng. Mech.* 19 (2005) 459–475.
[24] C.T. Loy, J.N. Lam, J.N. Reddy, Vibration of functionally graded cylindrical shells, *Int. J. Mech. Sci.* 41 (1999) 309–324.
[25] C.P. Wu, Y.H. Tsai, Asymptotic DQ solutions of functionally graded annular spherical shells, *Eur. J. Mech. A Solid* 23 (2004) 283–299.
[26] I. Elishakoff, C. Gentilini, E. Viola, Forced vibrations of functionally graded plates in the three-dimensional setting, *AIAA J.* 43 (2005) 2000–2007.
[27] I. Elishakoff, C. Gentilini, E. Viola, Three-dimensional analysis of an all-around clamped plate made of functionally graded materials, *Acta Mech.* 180 (2005) 21–36.
[28] B.P. Patel, S.S. Gupta, M.S. Loknath, C.P. Kadu, Free vibration analysis of functionally graded elliptical cylindrical shells using higher-order theory, *Compos. Struct.* 69 (2005) 259–270.
[29] S. Abrate, Free vibration, buckling, and static deflection of functionally graded plates, *Compos. Sci. Technol.* 66 (2006) 2383–2394.
[30] R.K. Bhangale, R.K. Ganesan, C. Padmanabhan, Linear thermo-elastic buckling and free vibration behavior of FG truncated conical shell, *J. Sound Vib.* 292 (2006) 341–371.
[31] A.M. Zenkour, Generalized shear deformation theory for bending analysis of functionally graded plates, *Appl. Math. Model.* 30 (2006) 67–84.
[32] J.L. Pelletier, S.S. Vel, An exact solution for the steady-state thermoelastic response of functionally graded orthotropic cylindrical shells, *Int. J. Solids Struct.* 43 (2006) 1131–1158.
[33] R.A. Arciniega, J.N. Reddy, Large deformation analysis of functionally graded shells, *Int. J. Solids Struct.* 44 (2007) 2036–2052.
[34] C.M.C. Roque, A.J.M. Ferreira, R.M.N. Jorge, A radial basis function for the free vibration analysis of functionally graded plates using refined theory, *J. Sound Vib.* 300 (2007) 1048–1070.
[35] A.H. Sofiyev, The buckling of functionally graded truncated conical shells under dynamic axial loading, *J. Sound Vib.* 305 (2007) 808–826.
[36] J. Yang, H.S. Shen, Free vibration and parametric resonance of shear deformable functionally graded cylindrical panels, *J. Sound Vib.* 261 (2007) 871–893.
[37] C. Shu, *Differential Quadrature and Its Application in Engineering*, Springer, Berlin, 2000.
[38] C. Bert, M. Malik, Differential quadrature method in computational mechanics, *Appl. Mech. Rev.* 49 (1996) 1–27.
[39] E. Viola, F. Tornabene, Vibration analysis of damaged circular arches with varying cross-section, *Struct. Integr. Durab. (SID-SDHM)* 1 (2005) 155–169.
[40] E. Viola, F. Tornabene, Vibration analysis of conical shell structures using GDQ method, *Far East J. Appl. Math.* 25 (2006) 23–39.
[41] F. Tornabene, Modellazione e Soluzione di Strutture a Guscio in Materiale Anisotropo, PhD Thesis, University of Bologna—DISTART Department, 2007.
[42] F. Tornabene, E. Viola, Vibration analysis of spherical structural elements using the GDQ method, *Comput. Math. Appl.* 53 (2007) 1538–1560.
[43] E. Viola, M. Dilena, F. Tornabene, Analytical and numerical results for vibration analysis of multi-stepped and multi-damaged circular arches, *J. Sound Vib.* 299 (2007) 143–163.
[44] C. Shu, Generalized Differential-integral Quadrature and Application to the Simulation of Incompressible Viscous Flows Including Parallel Computation, PhD Thesis, University of Glasgow, 1991.
[45] R. Bellman, J. Casti, Differential quadrature and long-term integration, *J. Math. Anal. Appl.* 34 (1971) 235–238.
[46] R. Bellman, B.G. Kashef, J. Casti, Differential quadrature: a technique for the rapid solution of nonlinear partial differential equations, *J. Comput. Phys.* 10 (1972) 40–52.
[47] F. Civan, C.M. Sliepcevich, Differential quadrature for multi-dimensional problems, *J. Math. Anal. Appl.* 101 (1984) 423–443.
[48] C.W. Bert, S.K. Jang, A.G. Striz, Two new approximate methods for analyzing free vibration of structural components, *AIAA J.* 26 (1988) 612–618.
[49] S. Jang, C. Bert, A.G. Striz, Application of differential quadrature to static analysis of structural components, *Int. J. Numer. Meth. Eng.* 28 (1989) 561–577.
[50] C. Shu, W. Chen, On optimal selection of interior points for applying discretized boundary conditions in DQ vibration analysis of beams and plates, *J. Sound Vib.* 222 (1999) 239–257.
[51] G. Karami, P. Malekzadeh, Application of a new differential quadrature methodology for free vibration analysis of plates, *Int. J. Numer. Meth. Eng.* 56 (2003) 847–868.
[52] J.R. Quan, C.T. Chang, New insights in solving distributed system equations by the quadrature method—I. Analysis, *Comput. Chem. Eng.* 13 (1989) 779–788.
[53] J.R. Quan, C.T. Chang, New insights in solving distributed system equations by the quadrature method—II. Numerical experiments, *Comput. Chem. Eng.* 13 (1989) 1017–1024.
[54] C. Shu, W. Chen, H. Xue, H. Du, Numerical study of grid distribution effect on accuracy of DQ analysis of beams and plates by error estimation of derivative approximation, *Int. J. Numer. Meth. Eng.* 51 (2001) 159–179.